Long-Baseline Neutrino Experiment (LBNE) Project

Conceptual Design Report

Volume 1: The LBNE Project

October 2012

Contents

List of Figures

List of Tables

6 Experimental Capabilities

6.1 Overview

Pursuit of the primary science objectives for LBNE as described in Chapter **??** dictates the need for very large mass (10-100 kiloton-scale) neutrino detectors located at a distance of > 1000 km from the neutrino source [1]. A large mass coupled with a powerful beam and long exposures is required to accumulate enough neutrino interactions – $\mathcal{O}(1000)$ events – to make precision measurements of the parameters that govern the sub-dominant $\nu_\mu \rightarrow \nu_e$ oscillations. The LBNE reconfiguration study [2] determined that the Far Detector location at SURF provides an optimal baseline (1,300 km) for precision measurement of neutrino oscillations using a conventional neutrino beam from Fermilab, and offers the best sensitivity to CP violation, as shown in Figure 6–1.

The large cosmic-ray background in the Far Detector, due to its location at the surface, limits the physics capabilities of LBNE to measurements done with the neutrino beam from Fermilab. The constraints of beam timing (10 μsec proton pulse every 1.33 seconds), the beam direction, as well as the relatively high-energy (> 1 GeV) specific signatures of the beam neutrino events, which permit powerful rejection of cosmic ray backgrounds, are not available for the non-beam physics that could be enabled by a large LArTPC detector.

This chapter concentrates on the capabilities of LBNE to address the beam-based neutrino oscillation physics, the primary science objectives of the Project. However, additional information is also provided regarding the research capabilities (nucleon decay searches, supernova-neutrino and atmospheric-neutrino measurements), that would be enabled if it became possible to place the Far Detector underground, either by obtaining additional resources beyond those assumed in developing the conceptual design presented in this CDR, or in a later stage of the LBNE program. This chapter discusses the long-baseline neutrino oscillation measurements that the ten-kiloton surface Far Detector will make using the neutrino beam from Fermilab (also described in [1]. Additional information is provided regarding the research capabilities (nucleon decay searches, supernova-neutrino and atmospheric-neutrino measurements), that would be enabled if an opportunity arose to place the Far Detector deep underground underground. The “Fall 2010 Report from the Physics Working Group” [3]

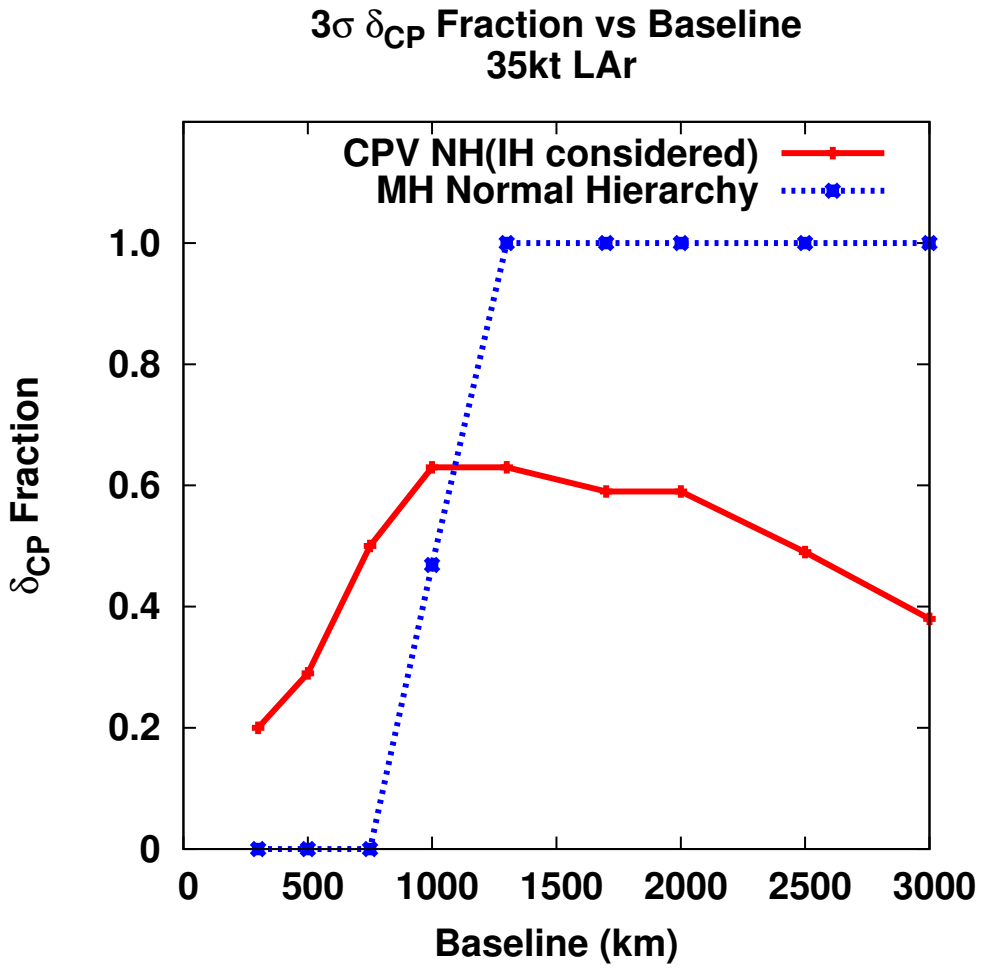

Figure 6–1: The fraction of δ_{cp} values for which CP violation and the mass hierarchy can be determined at the 3σ level or greater as a function of baseline. The LBNE beam design was optimized for each baseline. Projections assume $\sin^2 2\theta_{13} = 0.09$ and a 35 kton LArTPC as the far detector [1].

presents a detailed study of the more extensive physics capabilities of an LBNE implementation in which a 34-kiloton Far Detector is placed 4,580 feet underground and a near neutrino detector is deployed.

To meet the physics objectives of LBNE, the detector is required to have excellent particle identification capability over a wide range of particle energies from a few MeV to tens of GeV, corresponding to the energy range of particles that must be measured to fully reconstruct beam-neutrino events. To enable precision measurements of the parameters that govern $\nu_\mu \rightarrow \nu_e$ oscillations at the LAr-FD surface location, the far detector design and reconstruction techniques will need to reduce the cosmic-ray background to a level comparable to or below that of the beam backgrounds.

A substantial component of the background for ν_e charged-current (CC) interactions comes from neutral-current (NC) interactions where a π^0 is produced. The π^0 decays to two γs which shower electromagnetically and can thus fake the electron signal from a ν_e interaction. NC interactions in which a charged pion is produced are the predominant background for ν_μ CC interactions in which the pion mimics a muon. Therefore, to study neutrino-flavor oscillations with high precision, the LBNE Far Detector must be capable of high-efficiency, high-purity $e/\mu/\gamma$ and $\pi/K/p$ separation.

Time Projection Chambers (TPCs) are the detectors of choice for low-rate, large-volume, high-precision particle physics experiments due to their excellent 3D position resolution and particle identification in large volumes. In addition to detailed event topologies and measurements of particle kinematics, dE/dx measurements allow TPCs to unambiguously distinguish electrons, muons, photons, kaons, pions and protons (see Figure 6–2) over a wide range of energies.

The 10 kton LArTPC Far Detector, the LAr-FD, fulfills the high-mass requirement and provides excellent particle identification over a wide range of energies, as expected. In addition to identifying the flavor of neutrino interactions, measurements of the spectra of the oscillated neutrino signals over a wide energy range are required to enable precision measurements of the oscillation parameters. The best neutrino energy resolutions are obtained using charged-current quasi-elastic (CCQE) events in which the scattering of the neutrino is almost elastic; only a charged lepton and one or more nucleons emerge from the target nucleus. The charged lepton in CCQE events carries most of the energy of the neutrino. Final State Interactions (FSI) inside the nucleus will alter the expected nucleon types and spectrum. Measurements of this effect in a detector with an argon target nucleus, would help improve the neutrino energy resolution for all CC events in the LAr-FD. Information on FSI in neutrino interactions on argon will be available from the ArgoNeuT and MicroBooNE [4] experiments, and, if sufficient resources are found to construct a near neutrino detector for LBNE, this detector would be able to make these measurements over precisely the energy regime of LBNE. The LAr-FD photon-detection system is integrated with the TPC to detect scintillation light from particle interactions in order to (1) determine the exact start time of the drift, and (2) enable the localization of cosmic-ray muons to reduce backgrounds

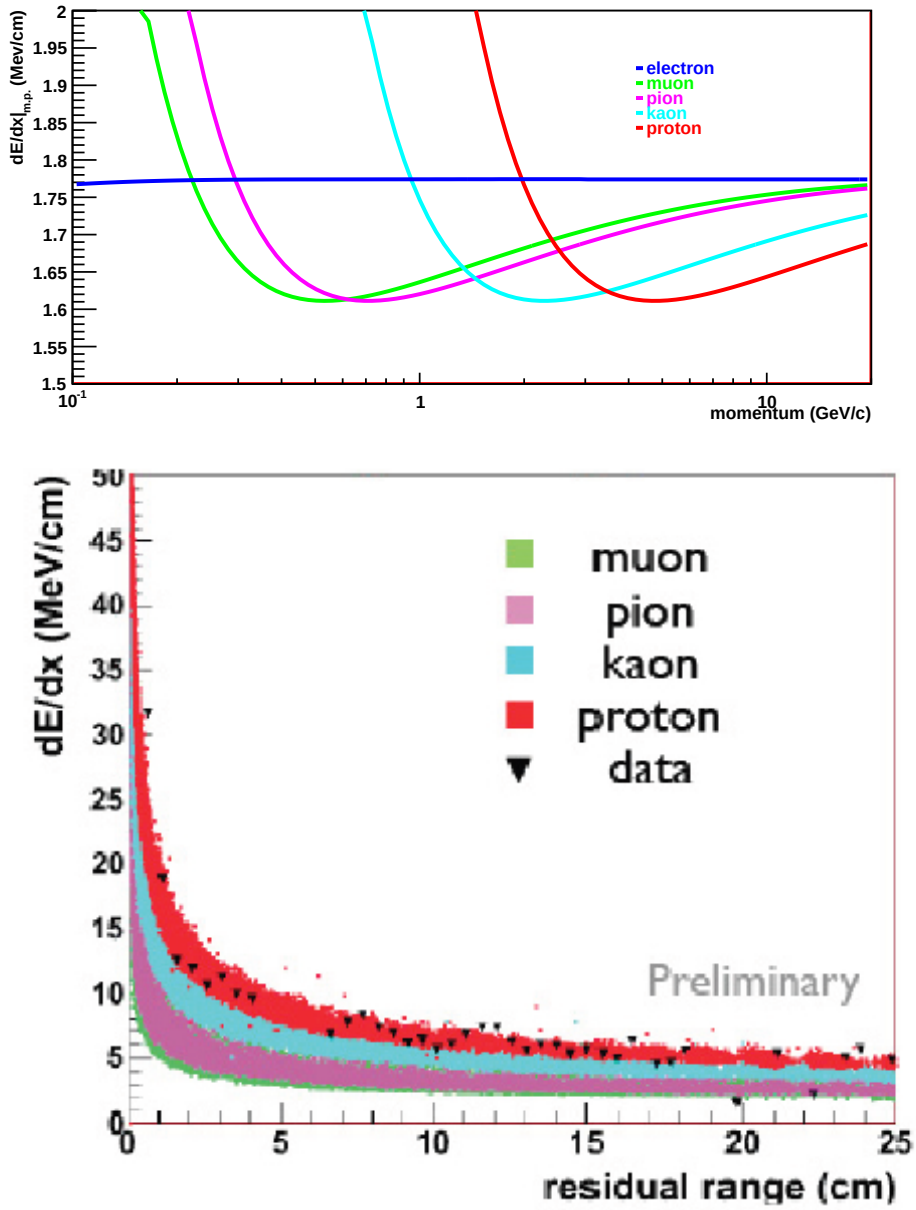

Figure 6–2: Distributions of dE/dx values for different charged particle species from a GEANT4 simulation of a liquid Argon TPC. The top plot is the most probable value of dE/dX vs particle momentum. The bottom plot is the value of dE/dx versus residual range from a GEANT4 simulation. The points are proton dE/dx measurements obtained from ArgoNEUT.

within the neutrino-beam spill window. The "LBNE Case Study Report for a Liquid Argon TPC" [5] has further details on the performance metrics of the LAr-FD.

To measure beam neutrino oscillations with the far detector, accurate predictions of the unoscillated neutrino flux spectrum are required. At the near site, an array of detectors just downstream of the absorber measures the energy spectrum and transverse profile of the muons that pass through the absorber. These muons come from the same pion and kaon decays that generate the neutrino beam, and therefore can be used to provide constraints on the unoscillated neutrino flux spectrum.

6.2 Accelerator-based Long-Baseline Neutrino Oscillations

The primary scientific objective for LBNE is the precision measurement of the parameters that govern neutrino oscillations over a long baseline, exceeding 1,000 km. Neutrino oscillations are described by the Pontecorvo-Maki-Nakagawa-Sakata (PMNS) leptonic mixing matrix [6]. Table 6–1 summarizes the current values of the neutrino oscillation parameters obtained from a global fit to experimental data [7]. A comparison to the equivalent mixing-parameter values in the quark CKM mixing matrix is also shown [6]. Clearly, the neutrino mixing parameters are not known nearly as precisely as are those in the quark sector.

Table 6–1: Best fit values of the neutrino mixing parameters in the PMNS matrix (assumes normal hierarchy) and comparison to the equivalent values in the CKM matrix from [7,6]. Δm^2 is defined as $m_3^2 - (m_1^2 + m_2^2)/2$.

Parameter	Value (neutrino PMNS matrix)	Value (quark CKM matrix)
θ_{12}	$34 \pm 1^\circ$	$13.04 \pm 0.05^\circ$
θ_{23}	$38 \pm 1^\circ$	$2.38 \pm 0.06^\circ$
θ_{13}	$8.9 \pm 0.5^\circ$	$0.201 \pm 0.011^\circ$
δm^2	$+(7.54 \pm 0.22) \times 10^{-5}$ eV^2	
$\lvert\Delta m^2\rvert$	$(2.43^{+0.10}_{-0.06}) \times 10^{-3}$ eV^2	$m_3 >> m_2$
δ_{CP}	$-170 \pm 54^\circ$	$67 \pm 5^\circ$

The observation of $\nu_\mu/\bar{\nu}_\mu \rightarrow \nu_e/\bar{\nu}_e$ oscillations in the neutrino-energy region from 0.5 to 5 GeV at 1,300 km, and measurement of their characteristics, would enable the unambiguous determination of the neutrino mass hierarchy and the measurement of δ_{cp}, the CP phase. Figure 6–3 shows the $\nu_\mu \rightarrow \nu_e$ oscillation probability (colored curves) at 1,300 km for $\sin^2 2\theta_{13} = 0.1$ and various values of the CP violating phase δ_{cp}. A detailed GEANT4 [8] simulation (see Figure 6–4) of the LBNE beamline, described in Volume 2 of this CDR, is used to estimate the neutrino flux at the far detector.

Table 6–2 lists the neutrino-interaction rates for all three known species of neutrinos as

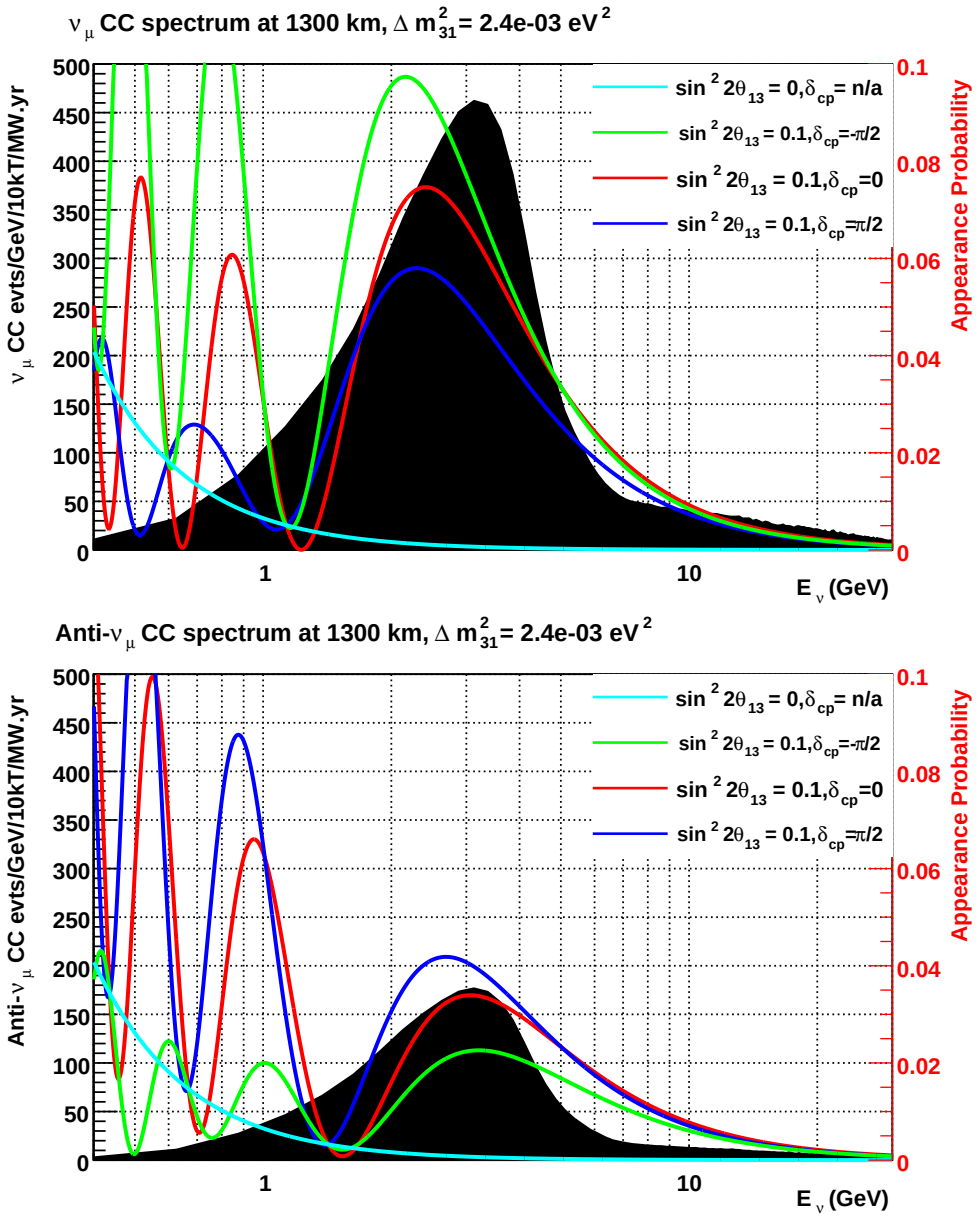

Figure 6–3: The $\nu_\mu \to \nu_e$ (top) and $\bar{\nu}_\mu \to \bar{\nu}_e$ (bottom) oscillation probabilities at 1,300 km for $\sin^2 2\theta_{13} = 0.1$ and normal hierarchy. The colored curves are for various values of the CP violating phase δ_{cp}. The cyan curve shows the ν_e appearance probability from the solar oscillation term only. The black histograms are the unoscillated ν_μ and $\bar{\nu}_\mu$ CC spectrum at 1300km from the low-energy (LE) beam tune.

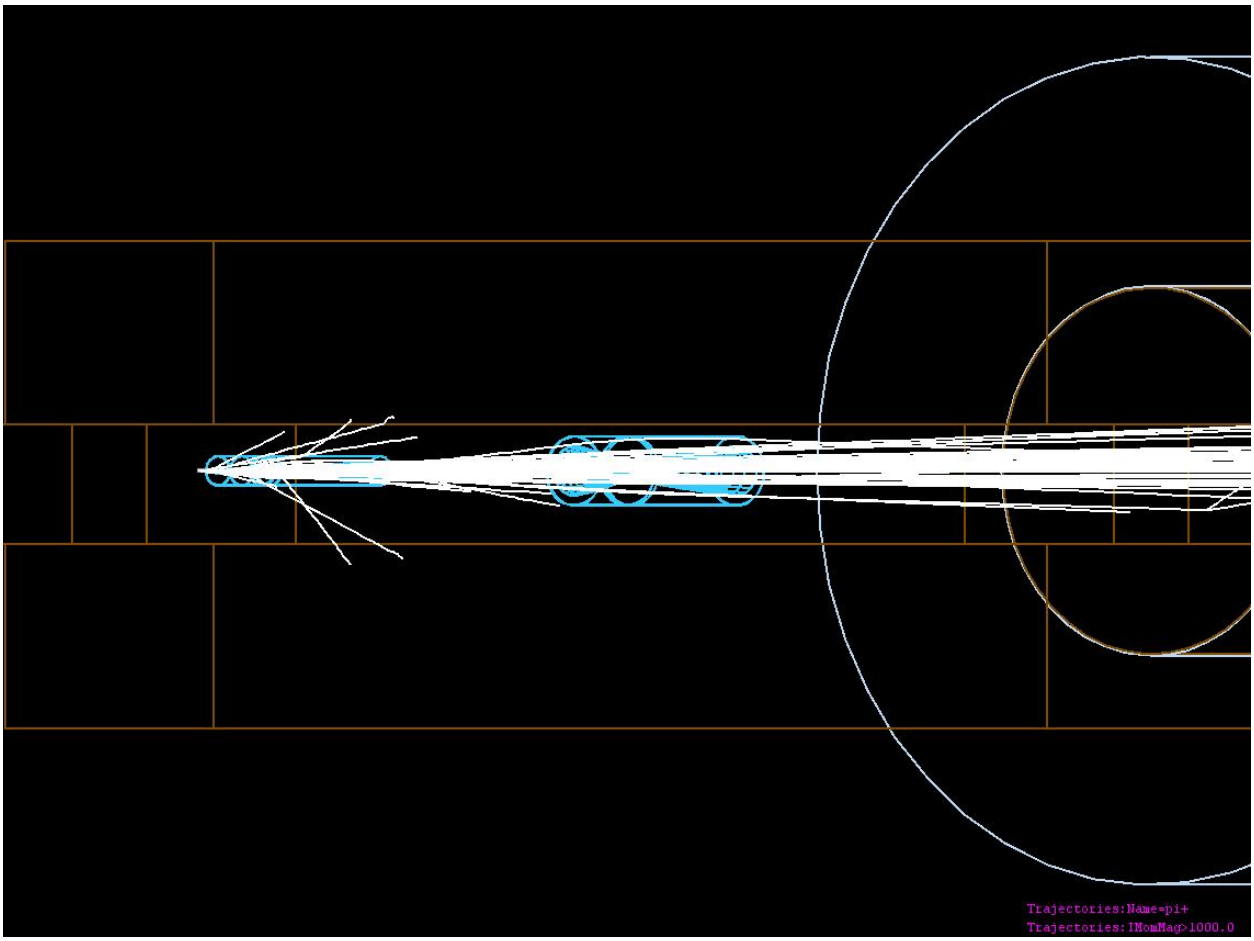

Figure 6–4: The GEANT4 simulation of the LBNE beamline. The 120 GeV proton beam is incident from the left. The NuMI horns are drawn in blue. The white lines are π^+ tracks with momenta > 1 GeV emerging from the target and entering the decay pipe at right.

expected at the LBNE Far Detector site. A tunable beam spectrum, obtained by varying the distance between the target and the first focusing horn (Horn 1), is assumed. The concept is illustrated in Figure 6–5, and examples of three possible beam tunes are shown in Figure 6–6.

Table 6–2: ν_μ, ν_τ, ν_e interaction rates per 10 kton.MW.yr (10^{21} protons-on-target) at the Far Detector site in LBNE for different beam tunes obtained by moving the target w.r.t. horn 1. Normal hierarchy, $\sin^2 2\theta_{13} = 0.1$. The rates are integrated in the region 0.5-20 GeV. The first column of numbers is the unoscillated ν_μ total charge-current interaction rate. The second column of numbers is the rate of ν_μ CC interactions expected given $\nu_\mu \to \nu_\mu$ oscillations.

Target Position	ν_μ CC	ν_μ CC osc	ν_μ NC	ν_e CC beam	$\nu_\mu \to \nu_e$ CC	$\nu_\mu \to \nu_\tau$ CC
-0.35 m (LE tune)	1.9K	720	420	29	80	9
-1.5 m (ME tune)	3.4K	2.2K*	764	35	97	44*
-2.5 m (HE tune)	4.1K	3.2K*	940	28	79	65*

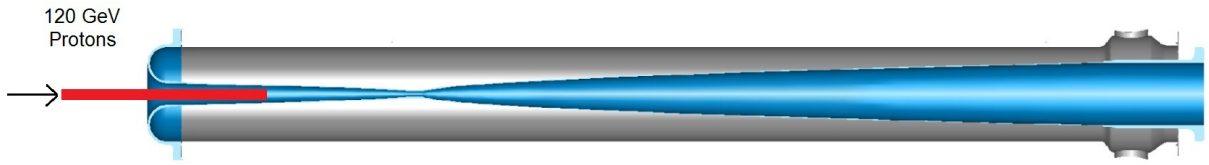

Figure 6–5: Configuration of movable target in Horn 1 to enable tuning of the beam. The horn has a double parabolic inner conductor (gray). The graphite target (red) is shown here partially inserted into Horn 1 in the Low-Energy (LE) beam tune position.

6.2.1 Measurement of the Unoscillated Neutrino Flux at the Near Detector Complex

Precise measurement of the parameters governing beam-neutrino oscillations at the Far Detector depends on comparison of the observed ν_μ or ν_e spectra with accurate predictions of the unoscillated spectra (flux and cross-section). The science and strategy for a long-baseline neutrino experiment near detector is detailed in [9].

Modern long-baseline experiments with near neutrino detectors, such as MINOS [10], are able to predict the unoscillated spectra and backgrounds at the Far Detector with a precision of 5% or better. The LBNE conceptual design does not include a high precision near neutrino detector. An overview of previous $\nu_\mu \to \nu_e$ experiments lacking near neutrino measurements [9] indicates that the beam systematic uncertainty on the ν_e appearance signal varies from 5% (NOMAD) to 14% (BNL E776). The MiniBooNE experiment [**?**], for example, achieved a systematic uncertainty on the unoscillated flux of 9% using target hadron-production data to constrain the beamline simulation. The LBNE NDC comprises a beamline-measurements system (BLM) that will be used to extract a measurement of the LBNE unoscillated neutrino flux using the same technique that was used in NuMI [11]. The

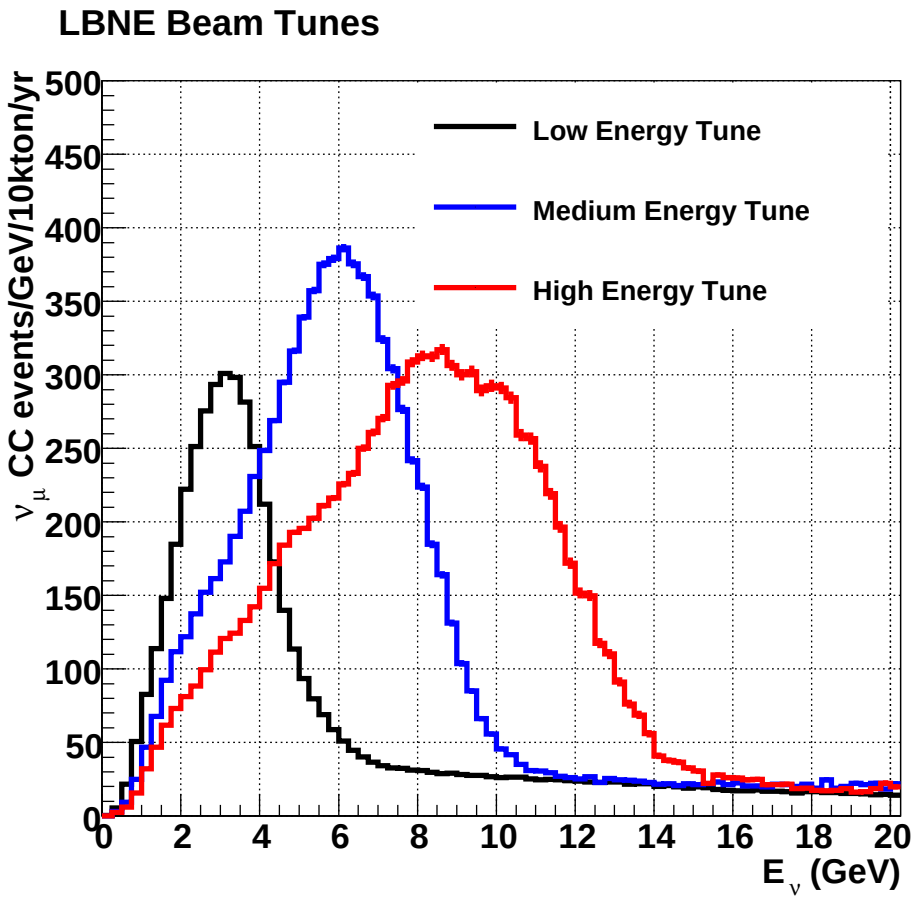

Figure 6–6: LBNE beam tunes produced by moving the target with respect to Horn 1. The default low-energy beam tune (black)is with the target partially inserted into Horn 1 as shown in Figure 6–5. Higher energy beam tunes can be obtained by moving the target out of Horn 1. For example, the medium energy tune (blue) is obtained by moving the target 1.5 m upstream of Horn 1. The highest energy tune available (red) is produced when the target is moved 2.5m upstream of Horn 1 - which is the maximum displacement of the target possible with the current carrier design. The beam is assumed to be 708 kW with 6.5×10^{20} protons-on-target/year

BLM system measures the flux of muons emerging from the neutrino beamline downstream of the absorber. Since the muons originate from the same hadron decays that produce ν_μ, the ν_μ flux can be extrapolated from measurements of the associated muons. The BLM is designed to measure the muon flux from the decays of $\pi^\pm \to \mu^\pm \nu_\mu$ and $K^\pm \to \pi^\pm \mu \nu_\mu$. The different detectors that comprise the NDC BLM are described in detail in Volume 3 of this CDR.

The following subsections describe the three techniques LBNE will use to obtain accurate simulations of its neutrino flux. The LBNE NDC plans to combine data from the NuMI beamline experiments such as MINOS and MINERνA with updated target hadron-production data and muon flux measurements from the LBNE BLM systems. Based on experience with current measurements from NuMI/MINOS, NA49 and expected updated hadron-production measurements from the NA61/Shine and MIPP experiments, it is expected that the LBNE unoscillated neutrino fluxes can be conservatively predicted to $\sim$10%. In-situ LBNE BLM measurements of the muon flux are expected to further improve the beamline simulation and predictions. For the $\nu_\mu \to \nu_e$ oscillation analysis, the oscillated ν_μ spectrum observed in the Far Detector can be used to further reduce the beam uncertainty on the ν_e appearance signal to $\sim$5%.

6.2.1.1 Beamline Simulation Tuning using NuMI Experiments

The LBNE beamline (described in Volume 2 of this CDR) is very similar to the NuMI beamline in design. The target and focusing horns are identical and in fact the only major difference is in the dimensions of the hadron decay pipe. (The length and diameter of the NuMI decay pipe are 675 m and 2 m, respectively, whereas LBNE's will be 204 m and 4 m.) The LBNE beamline simulation is therefore based on NuMI's, which has been tuned using MINOS near detector data at different beam energies, as shown in Figure 6–7.

The tuning involves reweighing the p_t, p_z distribution of the parent hadrons from the proton beam target and varying the production ratios of the different hadrons from the target as shown in Figure 6–8 [10]. In addition, the horn focusing and some cross section parameters are allowed to vary within modeling uncertainties.

As a result of the tuning, the NuMI simulation is able to model the MINOS near detector ν_μ and $\bar{\nu}_\mu$ spectra to better than 10% in the energy region from 0.5 to 10 GeV. The more finely segmented MINERνA detector [12], located upstream of the MINOS near detector, will carry out even more precise measurements of the unoscillated NuMI beam flux and is expected to further constrain the simulation of the NuMI beam. MINERνA data will also provide information on the ν_e component of the beam.

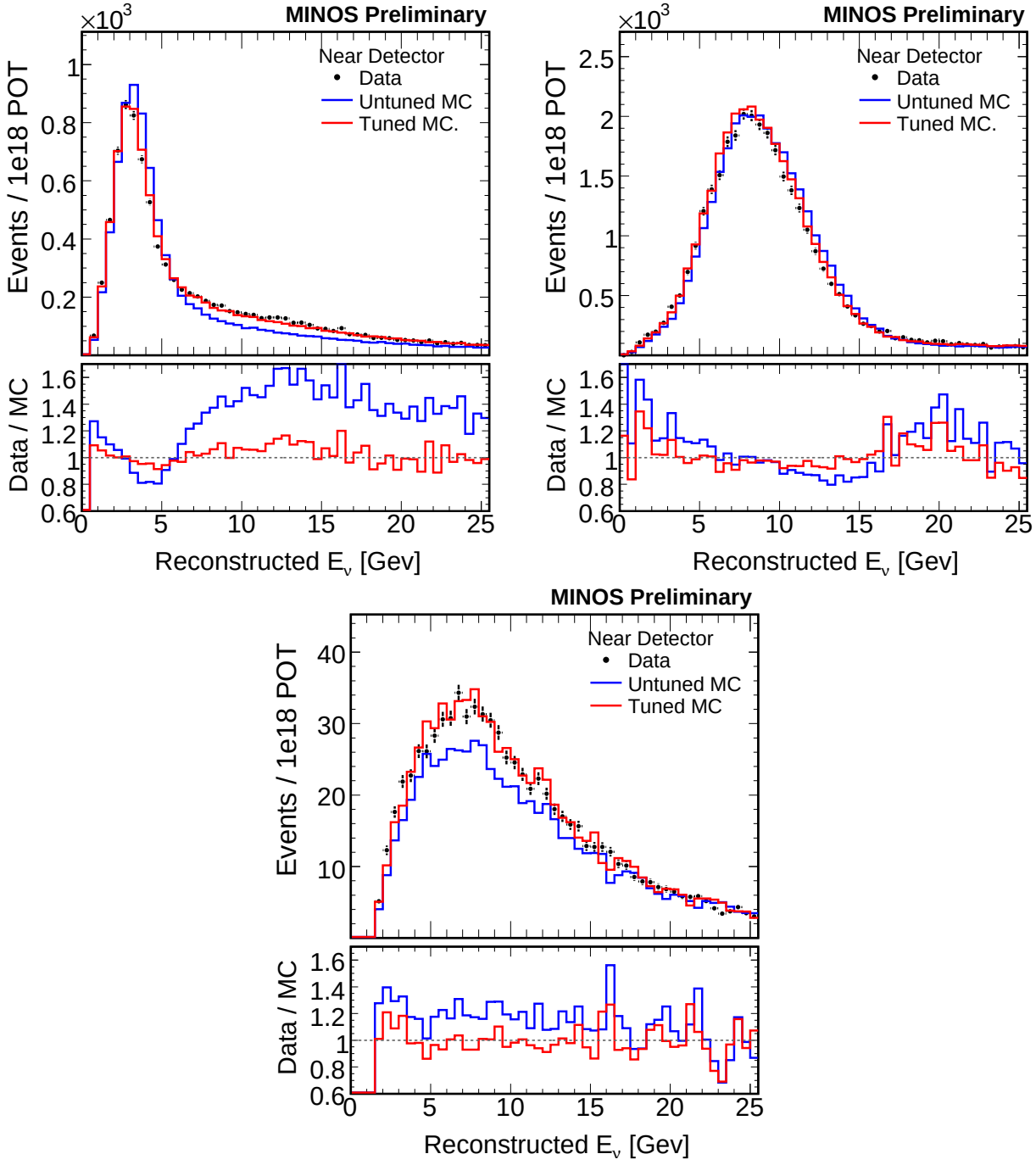

Figure 6–7: The MINOS near detector event spectra and the tuned MC predictions for the ν_μ CC signal from the low-energy tune (top left), the high-energy tune (top right) and $\bar{\nu}_\mu$ CC signal from the low-energy tune (bottom). The black data points with error bars represent experimental data from the MINOS near neutrino detector; the blue histogram shows the default FLUKA 2008 [13,14] MC and the red histogram shows the tuned MC.

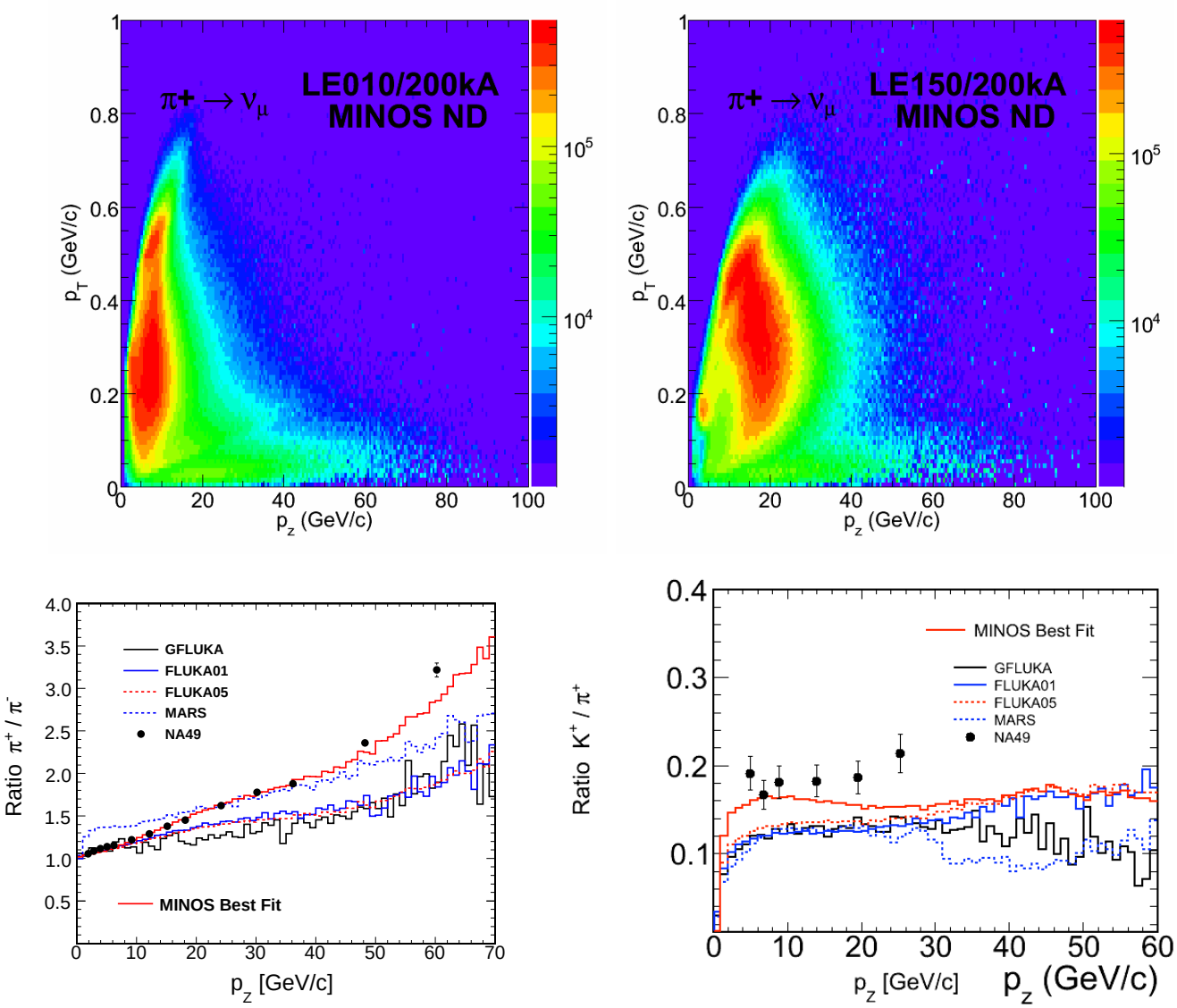

Figure 6–8: Tuning the MINOS MC to agree with the MINOS near detector and muon monitor data involves reweighing the p_t, p_z distribution of different beam tunes (top) of the hadrons produced from the target, varying the relative amount of different hadrons produced like the π^+/π^- ratio (bottom left) and the K^+/π^+ ratio (bottom right) to agree with the data from the near detector measurements. The tuned MC fit shown here (solid red line) is obtained by fitting the near neutrino detector data. Hadron production data from the NA49 experiment are shown as black points with error bars overlaid with the predictions from different simulation models, shown as colored histograms.

6.2.1.2 External Target Hadron Production Data

Measurements of hadron production from graphite targets in other experiments are critical to achieve a high-precision simulation of the neutrino flux from the LBNE beamline. In Figure 6–8, hadron-production data from the NA49 experiment [15] are compared to the tuned NuMI MC and found to be in good agreement. In fact the NuMI beamline tune revealed that the majority of the discrepancy between the MC and near detector neutrino data could be attributed to the inaccuracy of the hadron-production models in the 2005 version of the FLUKA MC [13,14]. For LBNE, additional data from the NA61/Shine experiment [16] and the MIPP experiment [17] will be used to further improve the accuracy and precision of the LBNE beamline MC simulation.

6.2.1.3 In-situ Muon Flux Measurements

NuMI employs a beamline measurement system to (indirectly) measure the neutrino flux independently of its near neutrino detector. The technique involves extrapolating the neutrino flux from muon data collected by a system that monitors the muon flux in the tertiary beam downstream of the decay pipe. The charge in the NuMI muon monitors is measured using different beam tunes and horn currents as shown in Figure 6–9. LBNE's BLM design is based on NuMI's and uses the same technique [11], but provides significant improvements and is expected to validate and enhance the tuned simulations discussed above.

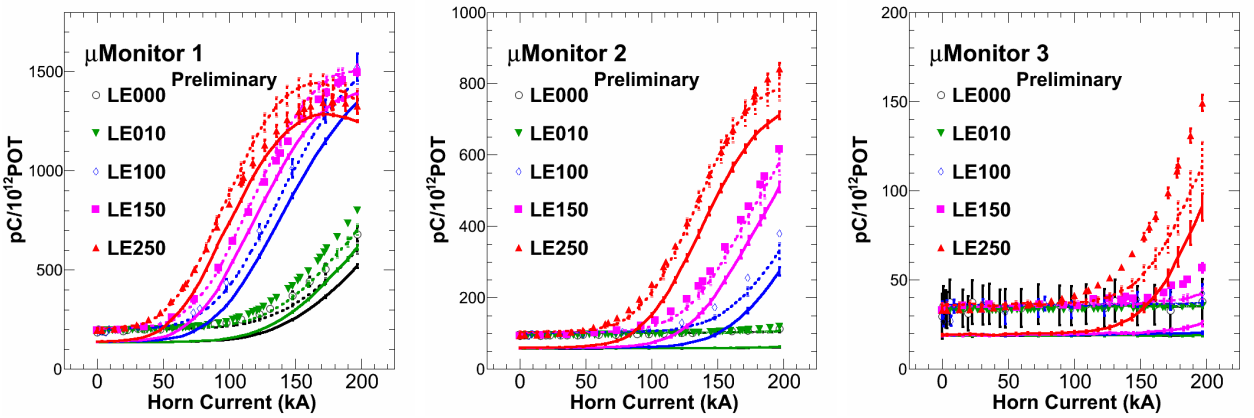

Figure 6–9: The NuMI muon monitor data [11] obtained by varying the beam tunes and varying the horn current. The data is shown as the solid colored points and the default MC prediction is shown as solid lines. The tuned MC prediction is shown as dashed lines and points. The different beam tunes are obtained by moving the target with respect to Horn 1. The tunes are target at -35cm (LE000), -45cm (LE010), -100cm (LE100), -150cm (LE150), and -250cm (LE250).

The NuMI muon monitors [18] are placed in alcoves at three separate locations downstream of the NuMI absorber to sample different portions of the muon spectrum (see Figure 6–10).

Each monitor consists of a 9 × 9 pad ion-chamber array and samples the muon-beam profile to a radius of approximately 1 m. The alcoves are separated by layers of rock to range out muons so that the monitors in each alcove sample different portions of the muon spectrum. The muons must have initial momenta of 5, 12 and 24 GeV, respectively, to be detected at the three locations.

The LBNE BLM will sample the muon flux at six different locations downstream of the LBNE absorber. The locations are separated by walls of steel "blue blocks" that provide several depths at which to monitor the muons as they range out. The BLM employs three different detector technologies; the different detectors are distributed among the locations as shown in Figure 6–10. The technologies consist of:

- variable-pressure gas Cherenkov counters
- 5 × 5 ion-chamber array
- stopped-muon counters

NuMI uses a FLUKA05/GEANT3 simulation of its beamline to predict both the muon flux in each alcove and the neutrino beam spectrum in the neutrino detector. The simulation is tuned using the charge measurements in the muon monitors and utilizes the technique described in Figure 6–8, which is very similar to that used to tune the MC to the MINOS near detector data, described in Section 6.2.1.1.

The NuMI muon-monitor data and the corresponding simulation predictions are shown in Figure 6–9 [11]. The neutrino flux measurements obtained from the NuMI muon monitors and the systematic uncertainties are shown in Figure 6–11. The tuning of the NuMI beamline simulation using the NuMI muon-monitor measurements was limited by the lack of both accurate calibration data and estimates of the neutron and delta ray backgrounds in the ion chambers [11]. This is reflected in the estimate of the neutrino flux uncertainty, which is dominated primarily by background uncertainties. Target hadron-production uncertainties also contribute significantly to this uncertainty since reliable target hadron-production data were not available at the time.

The LBNE BLM consists of a variety of detector technologies that improve on the ion-chamber arrays used by NuMI. The system will provide redundant measurements and will include more accurate calibration of the chamber responses. Prototypes of the LBNE muon chambers are scheduled for installation in the NuMI beamline in 2013 in order to carry out simultaneous measurement of the muon and muon-neutrino fluxes and to better understand background estimates.

FIXME: *Anne got to here Friday 10/19 2pm; will continue!*

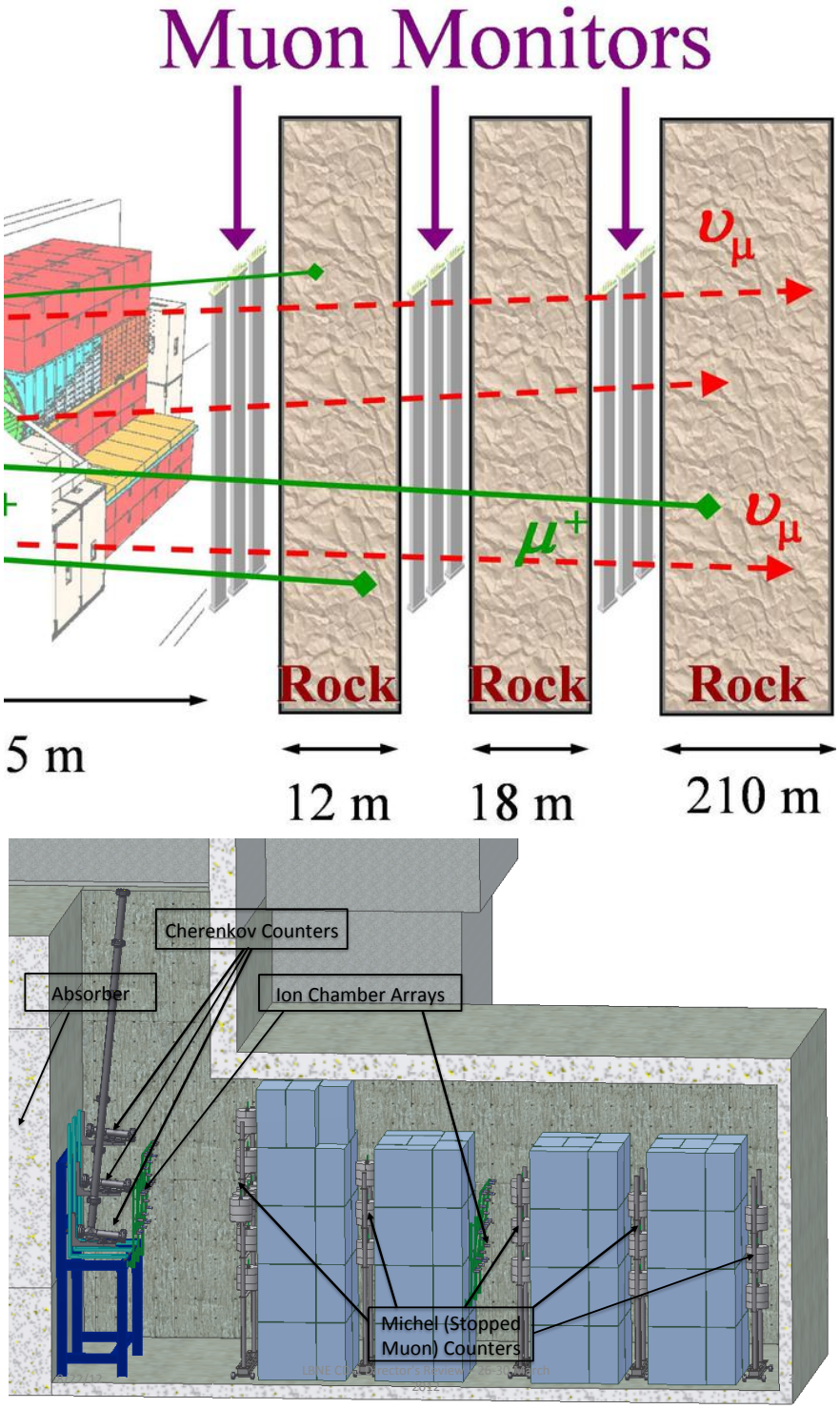

Figure 6–10: The NuMI muon beam measurement system (top) and LBNE BLM systems (bottom). The NuMI system comprises three detector alcoves each containing one array of 9×9 pad ionization chambers. The LBNE BLM system includes three different detector technologies distributed in six locations downstream of the absorber.

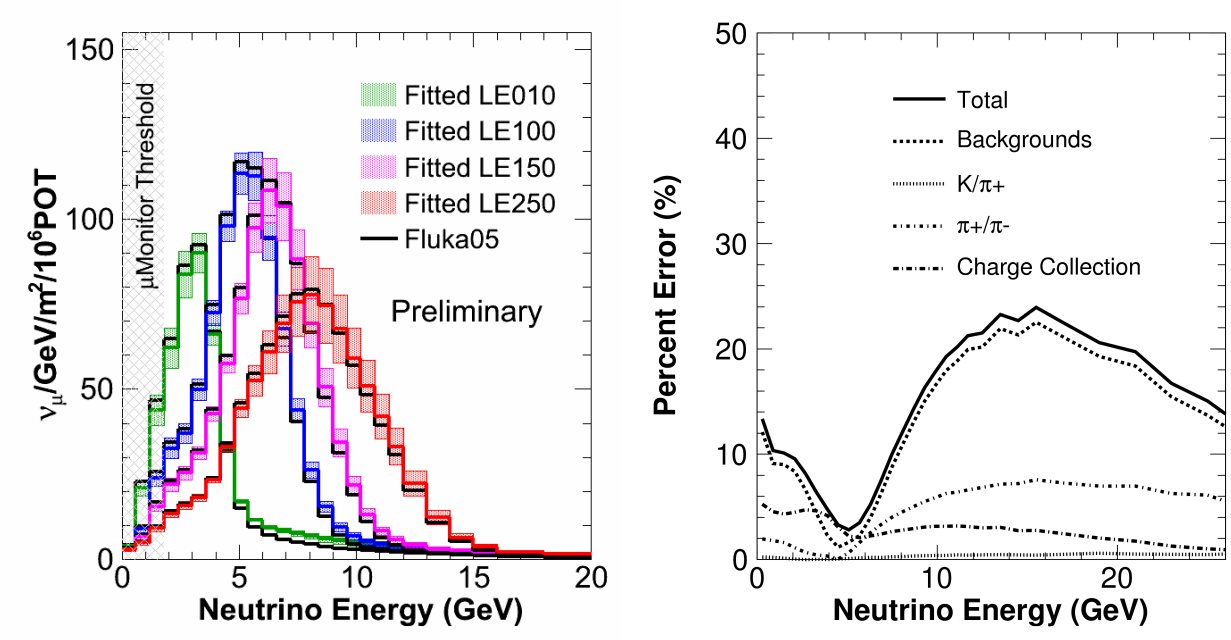

Figure 6–11: The NuMI flux prediction for 3 different beam tunes obtained by fitting the data in the 3 muon monitors is shown as the solid colored histograms (left). The black histogram is the initial FLUKA 2005 MC prediction. The colored bands represent the uncertainty on the flux prediction from the muon monitors. The shaded gray area represents the region of the NuMI flux that is not sampled by the muon monitors. The plot on the right shows the breakdown of the uncertainties on the flux prediction of the low energy beam.

6.2.2 Measurements of Mass Hierarchy and the CP-Violating Phase

A primary science objective of LBNE is to make precise measurements of the parameters that govern $\nu_\mu \rightarrow \nu_e$ oscillations. These parameters probe CP violation in the neutrino sector and determine the neutrino mass hierarchy. The sensitivity of the LAr-FD for ν_e appearance physics is primarily dependent on the signal efficiency for detecting electron-neutrino interactions and the background rejection of neutral current (NC) events and ν_μ charged current (CC) events in the range of 500 MeV to 5 GeV. NC events containing π^0s are the dominant source of background from NC interactions. The π^0 decays to two photons which convert to e^+e^- pairs and initiate an electromagnetic shower that can be difficult to distinguish from an electron shower. High particle identification efficiency and e/γ separation with high purity is required to distinguish ν_e CC from ν NC events. Excellent μ/e separation is also required to enable the distinction of ν_μ and ν_e CC interactions.

In addition to measurements of the CP parameters, LBNE will search for physics beyond the Standard Model with high-precision measurements of the parameters Δm^2_{32} and $\sin^2 2\theta_{23}$ in ν_μ and $\bar{\nu}_\mu$ long-baseline oscillations. These measurements require high-purity identification of ν_μ CC interactions, which requires high-precision separation of $\mu/\pi/p^+$. The strength of the LAr-FD is the ability to use detailed event topology, particle kinematics and dE/dx to differentiate ν_e, ν_μ CC and NC π^0 event classes with high purity and efficiency as illustrated in Figure 6–12.

The expected performance of the LAr-FD is extrapolated from the analysis results obtained from four independent studies of massive LArTPCs. The four studies are detailed in references [20], [21], [22] and [23], and are summarized in Table 6–3.

The most detailed LArTPC performance parameters to date were obtained from studies by the ICARUS collaboration [24] and the 2-km detector proposal for the T2K experiment [20]. The simulated geometry of the TPC for the 2-km T2K proposal is summarized in Table 6–3. This study is the only one to use fully automated 3D event reconstruction combined with dE/dx particle id and event kinematics in an automated analysis. The neutrino-event reconstruction and analysis were optimized to separate ν_μ CC and ν_μ NC separation, but did not include e/π^0 separation. As a result, the observed rate of 6.9% of NC events misidentified as ν_e CC is an over-estimate. A separate likelihood analysis of single electrons and π^0 interactions in the T2K 2-km LArTPC demonstrated that the single π^0 misidentification rate can be reduced to a few % using dE/dx alone, as shown in Figure 6–13. Therefore, the 6.9% NC misidentification rate could be greatly reduced by including e/π^0 separation in the analysis.

The last three studies in Table 6–3 comprise visual scans of simulated events in which researchers are trained to identify ν_e, ν_μ and NC π^0 interactions by studying event displays on an event-by-event basis. After training, the scanners are presented with a mixed sample of simulated events and asked to categorize them. Efficiencies are determined by comparing the scanners' results to the known event type. The selection efficiencies for signal-neutrino

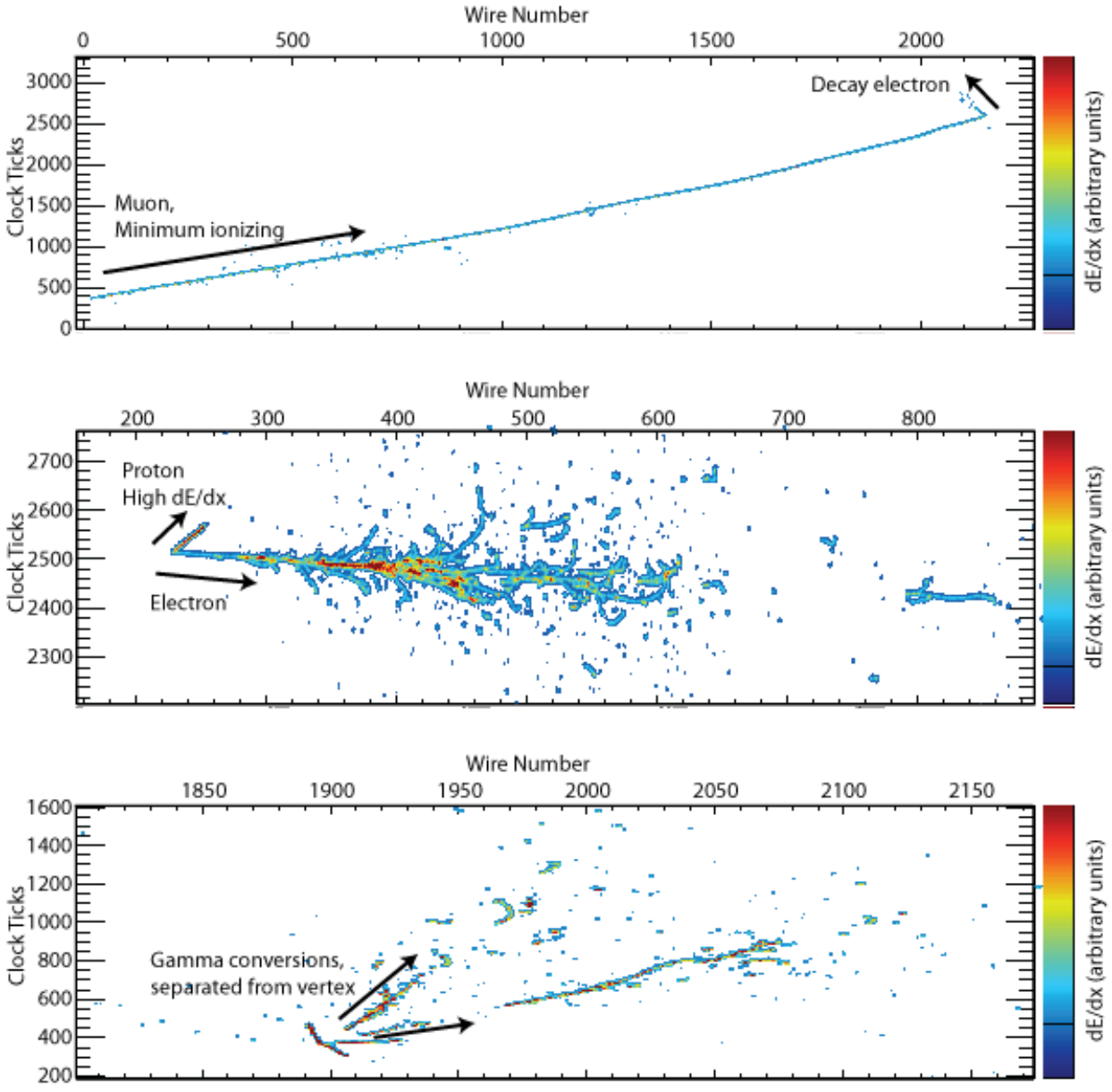

Figure 6–12: Examples of neutrino beam interactions in an LArTPC obtained from a GEANT4 simulation [19]. A CC ν_μ interaction with a stopped μ followed by a decay Michel electron (top), a CCQE ν_e interaction with a single electron and a proton (middle), an NC interaction which produced a π^0 that then decayed into two γ's with separate conversion vertices (bottom)

interactions and the rejection efficiencies for NC background, determined by the four studies summarized here, are shown in Table 6–4. There is general agreement between all four studies regarding the efficiency for identifying ν_e CC events in the few-GeV range; they find it to be between 70 and 95%. In addition, the reconstruction efficiency of ν_e CC as a function of neutrino energies has been found to be approximately flat for neutrino energies > 1 GeV, as

Table 6–3: Description of the LAr-TPC simulations used to determine the performance for beam neutrino interactions.

Study	TPC geometry	Analysis technique
T2K 2km proposal [20] (2005)	140 tons, 4.5m(w)x4.5m(h)x5m(l) 2 readout chambers, 2 planes/chamber 3mm/6.4m wire pitch/length 2.21m/1.1ms max drift distance/time	Fully automated reconstruction, event topology, $\mu/\pi^{\pm}/K/p^{+}$ dE/dX and event kinematics included in a Random Forest analysis
Tufts Visual Scan [21] (2006)	Unknown	Blind visual scan visible energy precuts topology only
FNAL Visual Scan [22] (2008)	2.5m(w)x2.5m(h)x2.5m(l) 1 readout chamber, 2 planes/chamber 5mm and 10mm wire pitch	Blind visual scan MC truth used in precuts topology and dE/dX included in a log-likelihood analysis
FNAL Visual Scan [23] (2011)	MicroBooNE TPC	Blind visual scan topology only

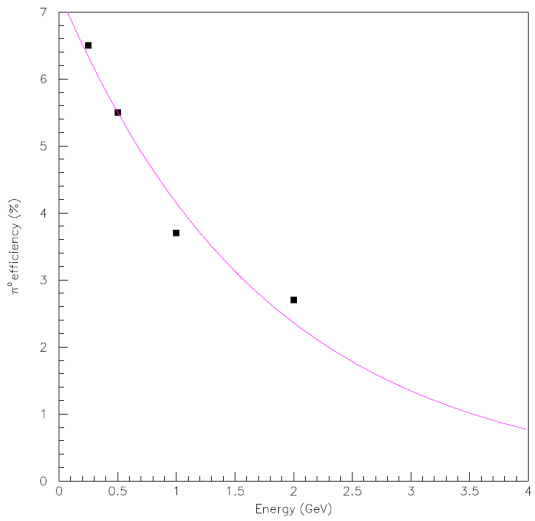

Figure 6–13: The electron mis-identification rate of single π^0 interactions as a function of the incoming π^0 energy [20].

shown in Figure 6–14. The misidentification rate of ν_μ CC events obtained from these studies is about 2%. Since optimized e/μ separation using dE/dx has not yet been implemented in these studies, the 2% ν_μ misidentification rate will be considered an upper limit.

A large variation is observed in the NC misidentification rate. The lowest rate was obtained by the visual scan study that included a crude dE/dx measurement combined with topology [22].

Table 6–4: Selection efficiencies for ν_e CC candidates and ν_e misidentification rates for ν_μ CC and ν_μ NC determined by various studies. The / symbol indicates samples where the event size was too small to draw meaningful conclusions.

Study	**Average** ν energy	**# events** studied	ν_e **CC** $\epsilon_{\rm select}$	ν_μ **CC** $\epsilon_{\rm mis-id}$	ν_μ **NC** $\epsilon_{\rm mis-id}$
T2K 2km proposal (2005)	0.25-4.0 GeV	2000	94.5%	2%	6.9%
Tufts Visual Scan (2006)	NOνA beam 1.5-4.5 GeV	450	$72 \pm 5\%$	/	$1.3 \pm 0.4\%$
FNAL Visual Scan (2008)	NOνA beam 0.5-3.5 GeV	4997	$92 \pm 9\%$	/	$0.6 \pm 0.1\%$
FNAL Visual Scan (2011)	Uniform 0.5-15 GeV	1501	$90 \pm 1\%$	$2.0 \pm 0.6\%$	$5 \pm 1\%$

The estimation of the NC misidentification rate is further complicated by the fact that only the last study in Table 6–4 simulated ν NC interactions with energies > 5 GeV. In the search for ν_e appearance by the MINOS experiment [25] – which has a beam-neutrino spectrum and ν_e-signal range very similar to LBNE's – it was observed that $\approx 50\%$ of the NC background in the 1–5 GeV signal region originated from NC inelastic interactions with neutrino energies >5 GeV. An example of the complicated topology of deep inelastic NC interactions is shown in Figure 6–15. Reliable estimates of the NC misidentification rate of such events are not available. Given the current knowledge of LArTPC performance from these studies, the LBNE NC misidentification rate is estimated to be between 2% (conservative) to 0.4% (aggressive), depending on how well e/π^0 separation techniques will perform in more complicated topologies.

For the neutrino-oscillation sensitivity calculations, information from these hand scans is used to set the detector-signal efficiencies and background-rejection efficiencies. Table 6–5 shows the range of ν_e selection efficiencies, background levels and neutrino energy resolutions from the hand scans in Table 6–4, along with the specific values chosen for the long-baseline oscillation-sensitivity projections.

Studies from ICARUS have estimated and measured single-particle energy resolutions in LAr. Below 50 MeV, the energy resolution of electrons is $11\%/\sqrt{E[MeV]} + 2\%$. As shown in Figure 6–16, the energy resolution of an electromagnetic shower with energy in the range (50–5000) MeV is $33\%/\sqrt{E(MeV)} + 1\%$ [26]. The energy resolution of hadronic showers in an LArTPC is $\approx 30\%/\sqrt{E(GeV)}$. A significant fraction of the ν_e CC signal in LBNE in the range of 1–6 GeV is non-quasi-elastic CC interactions with a large component of the visible energy in the hadronic system. From recent simulations of neutrino interactions in the region of 1–6 GeV it has been determined that $< E_{\rm lepton}/E_\nu > \approx 0.6$. For this reason, the

Table 6–5: Estimated range of the LAr-TPC detector performance parameters for the primary oscillation physics. Signal efficiencies, background levels, and resolutions are obtained from the studies described in this chapter (middle column) and the value chosen for the baseline LBNE neutrino-oscillation sensitivity calculations (right column). * For atmospheric neutrinos this is the mis-identification rate for < 2 GeV events, the mis-identification rate is taken to be 0 for > 2 GeV.

Parameter	**Range of Values**	**Value Used for LBNE Sensitivities**
For ν_e CC appearance studies		
ν_e CC efficiency	70-95%	80%
ν_μ NC mis-identification rate	0.4-2.0%	1%
ν_μ CC mis-identification rate	0.5-2.0%	1%
Other background	0%	0%
Signal normalization error	1-5%	1-5%
Background normalization error	2-15%	5-15%
For ν_μ CC disappearance studies		
ν_μ CC efficiency	80-95%	85%
ν_μ NC mis-identification rate	0.5-10%	0.5%
Other background	0%	0%
Signal normalization error	1-10%	5-10%
Background normalization error	2-20%	10-20%
For ν NC disappearance studies		
ν NC efficiency	70-95%	90%
ν_μ CC mis-identification rate	2-10%	10% *
ν_e CC mis-identification rate	1-10%	10% *
Other background	0%	0%
Signal normalization error	1-5%	under study
Background normalization error	2-10%	under study
Neutrino energy resolutions		
ν_e CC energy resolution	$15\%/\sqrt{E(GeV)}$	$15\%/\sqrt{E(GeV)}$
ν_μ CC energy resolution	$20\%/\sqrt{E(GeV)}$	$20\%/\sqrt{E(GeV)}$
E_{ν_e} scale uncertainty	under study	under study
E_{ν_μ} scale uncertainty	1-5%	2%

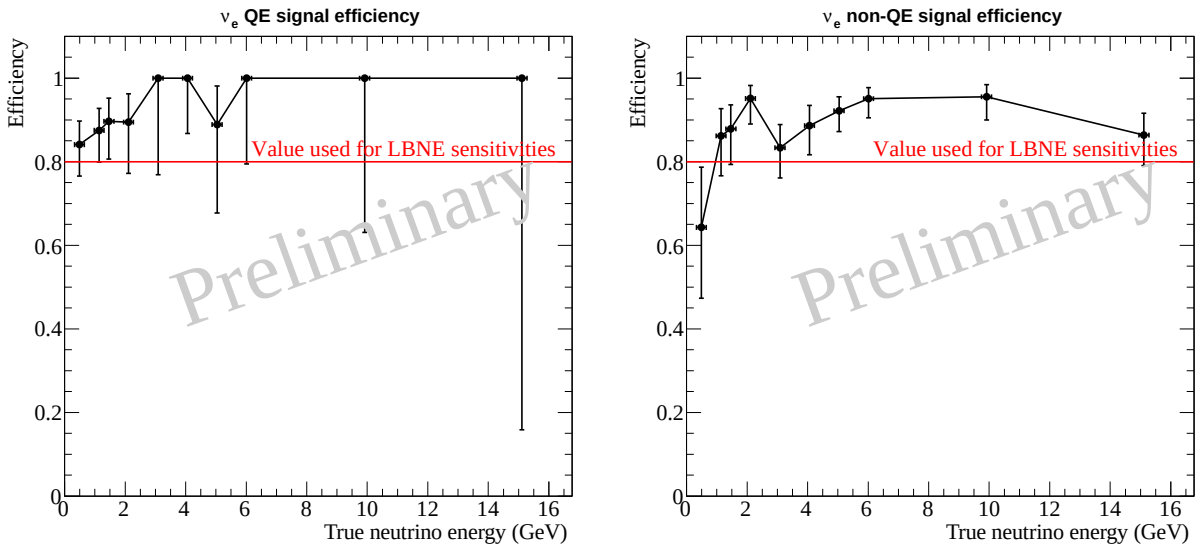

Figure 6–14: The efficiency, as determined by the 2011 Fermilab hand scan study [23] , of selecting ν_e CC quasi-elastic (left) and non-quasi-elastic(right) events.

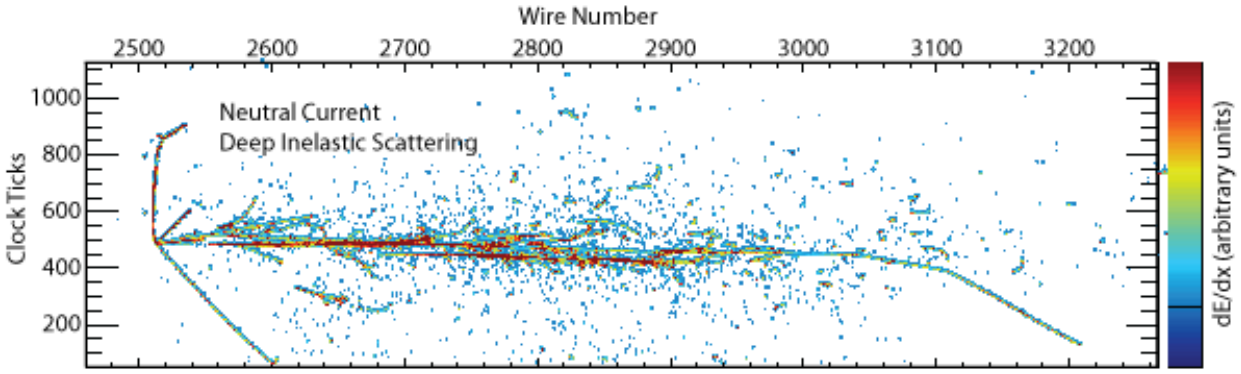

Figure 6–15: An example of a deep inelastic NC interaction in a LAr-TPC.

total electron-neutrino energy resolution for the neutrino-oscillation sensitivity calculation is chosen to be $15\%/\sqrt{E(GeV)}$. In a non-magnetized LArTPC the muon momentum can be obtained from range and multiple scattering. The muon-momentum resolution is found to be in the range $10-15\%$ [20] [27] for muons in the 0.5–3 GeV range. Therefore the total muon-neutrino energy resolution in LBNE is assumed to be $20\%/\sqrt{E(GeV)}$.

In five years of neutrino (antineutrino) running, assuming $\sin^2(2\theta_{13}) = 0.1$, $\delta_{CP} = 0$, and normal mass hierarchy, a total of about 180 (62) selected $\nu_e(\overline{\nu}_e)$ signal events in a 10 kton LAr-FD are expected with a 708-kW beam. Table 6–6 is a summary of the expected number of signal and beam background events for ν_e and $\overline{\nu}_e$ running for normal and inverted hierarchy. The spectrum of expected signal and background events is shown in Figure 6–17.

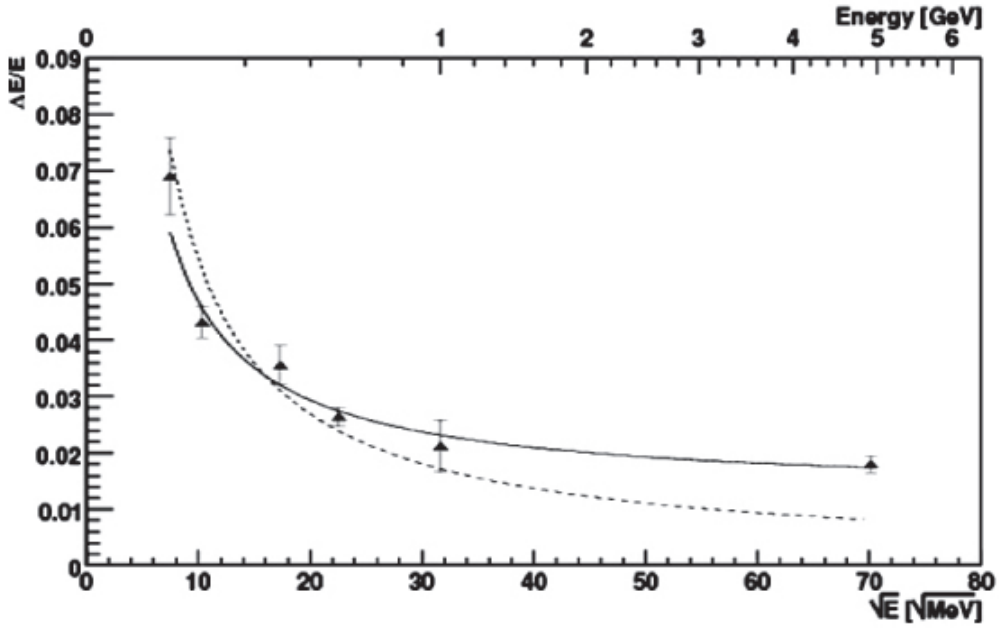

Figure 6–16: Resolution of electromagnetic showers from ICARUS [26]

A preliminary study of the expected non-beam background events expected from cosmic rays in the 10 kton LAr-FD located near the surface at SURF is detailed in [28]. The study simulated cosmic-ray interactions in the LAr-FD and focused on cosmic-ray induced signals from neutrons and muons that mimic electron-neutrino interactions such as electromagnetic cascades from knock-on electrons, muon Bremstrahlung, or hadronic cascades with electromagnetic components from photons and π^0s. Backgrounds from neutral hadron decays into electrons such as $K_L^0 \rightarrow \pi e \nu$ were also studied. The energy of the cascades was required to be in the range > 0.1 GeV. Initial studies indicate that a combination of simple kinematic and beam timing cuts will help in significantly reducing the cosmic-ray background event rate in the 10 kton LAr-FD. The most relevant kinematic variables considered to reduce the cosmic-ray backgrounds are: 1) Only electro-magnetic cascades with energies greater than 0.25 GeV are considered background since for the neutrino oscillation sensitivity calculations, only neutrino energies ≥ 0.5 GeV were considered, 2) $e^{\pm}$ background candidates are tracked back to the parent muon and the distance between the muon track and the point-of-closest-approach (PoCA) to the muon track is required to be > 10 cm, 3) The vertex of the $e^{\pm}$ shower is required to be within the fiducial volume of the detector which is defined as 30cm from the edge of the active detector, 4) The $e^{\pm}$ cascade is required to be within a cone around the beam direction which is determined from the angular distribution of the beam signal $e^{\pm}$ and the incoming neutrino beam, 5) it is assumed that em showers initiated by γ's and $\pi^0 \rightarrow \gamma\gamma$ can be effectively distinghuished from primary electron interactions using particle ID techniques such as dE/dX and the reconstructed event topology as shown in Fig-

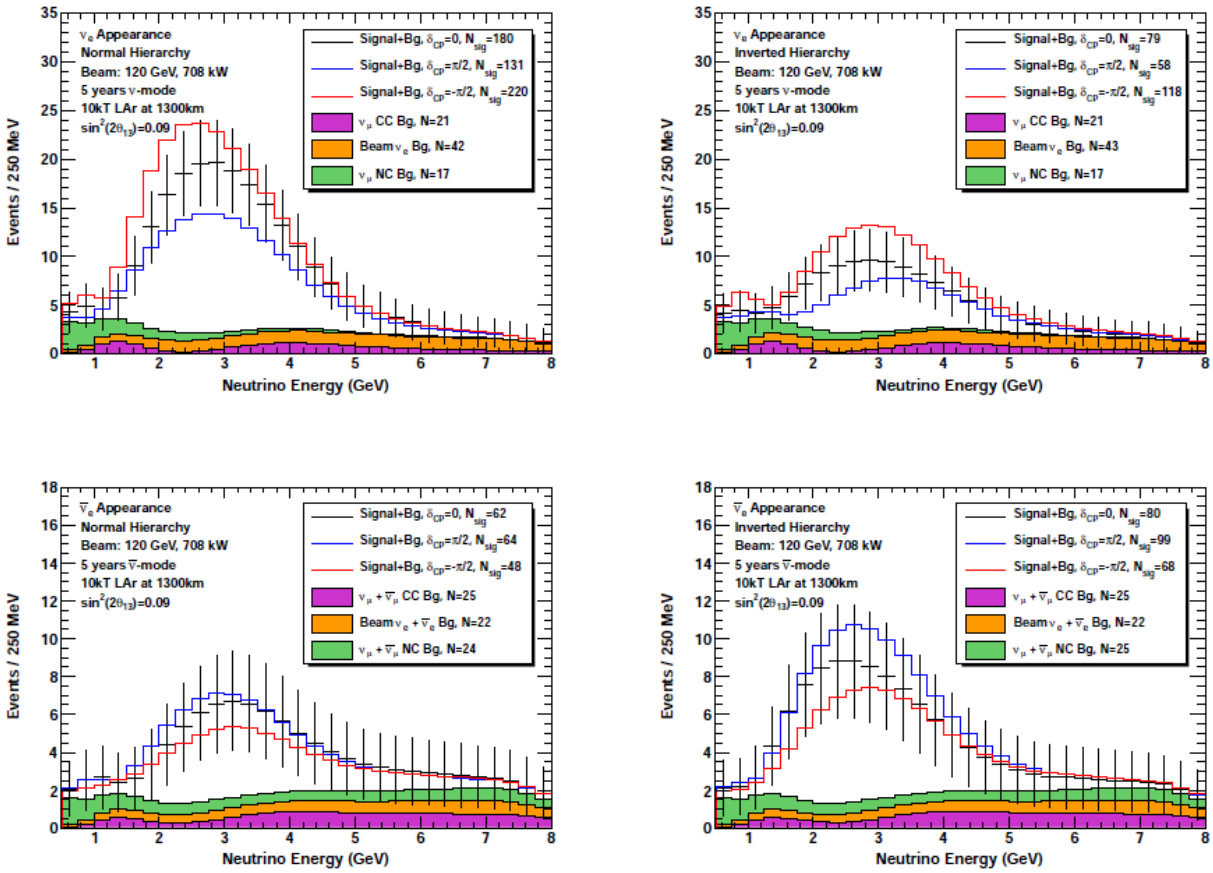

Figure 6–17: The expected spectrum of ν_e or $\overline{\nu}_e$ oscillation events in a 10 kton LArTPC for 5 years of neutrino (left) and antineutrino (right) running with a 708 kW beam assuming $\sin^2(2\theta_{13}) = 0.09$ for normal hierarchy (top) and inverted hierarchy (bottom). Backgrounds are displayed as stacked histograms.

ure 6–13, 6) events are timed with a precision of $\leq 1\mu$ seconds using the photon detection system which limits backgrounds to events occuring within the 10μ seconds of the beam spill. The result of applying these selection critiria to the em showers initiated by cosmics are summarized in Table **??**. The studies indicate that application of these selection critiria can potentially reduce the background from cosmic rays to a few events per year - mostly in the energy region < 1 GeV.

Although the preliminary studies outlined above indicate that it is feasible to reduce the cosmic-ray-induced background to a level below that of the beam background, a full simulation of the LAr-FD combined with advanced reconstruction techniques is needed for an accurate estimation of this background. Any such background will be accurately measured using off-spill data. It is assumed to be negligible when calculating sensitivities to neutrino-oscillation physics.

Table 6–6: Expected number of neutrino oscillation signal and background events in the energy range (0.5 - 8.0) GeV at the LAr-FD, assuming $\sin^2(2\theta_{13}) = 0.1$ and $\delta_{CP} = 0$, 10kt LAr-FD and 5 years of running with 6.5×10^{20} protons-on-target/year. The background from $\nu_\mu \rightarrow \nu_\tau \rightarrow \tau X \rightarrow e\bar{\nu}_e\nu_\tau X$ is estimated to be 2-3 events and is considered to be negligible.

	Signal Events	**Background Events**			
	ν_e	ν_μ CC	ν_μ NC	ν_e Beam	Total
Neutrino Normal Hierarchy	180	21	17	42	80
Neutrino Inverted Hierarchy	79	21	17	43	81
Anti-neutrino Normal Hierarchy	62	25	24	22	71
Anti-neutrino Inverted Hierarchy	80	25	25	22	72

Table 6–7: Cosmic ray backgrounds that produce electromagnetic showers in the detector and the expected event rate/yr after various selection critiria are applied from left to right. The initial background event rate is calculated assumning a 1.4 ms drift time per beam pulse, a beam pulse every 1.33 seconds and 2×10^7s of running/yr. The detector is assumed to be on the surface with 3m of rock overburden. Outer γ events are γ events that originate outside the detector and migrate into the active detector volume.

Background	$E_e > 0.25$ GeV	PoCA > 10cm	Fid > 30cm	Beam angle	e/γ PID	Beam timing
Muons in the detector						
$\mu^\pm \rightarrow e^\pm$	3.3×10^7	64	0	0	0	0
$\pi^0, K^0_L \rightarrow e^\pm$	940	170	170	68	68	0.5
$\pi^\pm, K^\pm, ... \rightarrow e^\pm$	7.4×10^5	2.7×10^3	43	17	17	0.12
$\pi^0 \rightarrow \gamma \rightarrow e^\pm$	1.6×10^5	2.0×10^4	1.9×10^4	7.5×10^3	150	1.1
$\mu \rightarrow \gamma \rightarrow e^\pm$	1.3×10^6	8.7×10^4	21	0	0	0
Outer $\gamma \rightarrow e^\pm$	4.7×10^5	4.6×10^3	530	210	4	0.03
Muons outside the detector						
Outer $\gamma \rightarrow e^\pm$	3.5×10^4	N/A	360	152	3	0.02
$\pi^0 \rightarrow \gamma \rightarrow e^\pm$	43	N/A	43	18	0.4	0.003
Cosmic neutrons from the surface						
Outer $\gamma \rightarrow e^\pm$	1.5×10^3	N/A	230	81	1.6	0.01
$\pi^0 \rightarrow \gamma \rightarrow e^\pm$	3.4×10^3	N/A	2.4×10^3	890	18	0.13
$n, \eta, \Sigma \rightarrow \gamma \rightarrow e^\pm$	140	N/A	110	37	0.75	0.05
Total $e^\pm$ background events/yr						
	3.7×10^7	2.2×10^5	2.2×10^4	9.0×10^3	270	2.0

The current LBNE design scope includes near detectors to measure the flux of muons from pion and kaon decays which can be used to estimate the unoscillated ν_μ neutrino flux from the beamline. The accuracy with which the unoscillated ν_μ, $\bar{\nu}_\mu$ and ν_e interaction rates can be estimated at the Far Detector in the absence of a high-precision near neutrino detector will depend on a combination of many inputs: 1) in-situ measurements of the absolute muon flux from the LBNE beamline, 2) external hadron-production measurements on graphite targets, 3) detailed beam simulations tuned to high accuracy using data from near detectors at existing experiments such as MINOS and NOνA which use the same NuMI focusing system, and 4) improved measurements of low-energy neutrino interaction cross-sections from the MiNERνA and MicroBOONE experiments. A study of the overall science and strategy for a long-baseline neutrino experiment near detector is presented in [9]. In addition, a detailed description of the techniques that will be deployed in LBNE to estimate the unoscillated neutrino flux at the far detector is discussed in Section 6.2.1.1. The uncertainty on the ν_e signal prediction at the far detector for the is estimated to be around 1% with a high precision near detector, and 5% without a near detector. The background uncertainties for the ν_e appearance signal is estimated to be 15% without a high precision near detector. The background uncertainties are driven by the flux uncertainties - which are estimated to be around 10% - and the detector particle identification and cross-section uncertainties. With a 10 kton LAr-FD, the statistical uncertainties on the signal – especially in the anti-neutrino mode – are expected to dominate the sensitivity.

Figure 6–18 shows the significance with which the mass hierarchy can be resolved and the determination of whether CP is violated ($\delta_{cp} \neq 0$ or π) as a function of the value of δ_{cp} for different fiducial-volume masses of LAr-FD. The bands indicate the sensitivity range corresponding to different assumptions on background and signal normalization uncertainties. The range of assumptions covers the estimates of background and signal uncertainties that could be achieved with the currently planned tertiary muon detectors monitoring the beam or with a high-accuracy near neutrino detector as detailed in [9].

For values of $\sin^2 2\theta_{13} = 0.092$, LBNE with a 10 kton LAr-FD can alone determine the mass hierarchy at the 3σ level for 75% of all values of δ_{cp} and will determine whether CP is violated for 25% of all δ_{cp} values at 2.5σ level [1]. A combination of the results from the LAr-FD with six years of NOνA running and the expected T2K data up to 2021 (5×10^{21} protons-on-target) [1] would enable a determination of both the mass hierarchy at $> 3.5\sigma$ for all values of δ_{cp} and the CP-violation at $\geq 3\sigma$ for 40% of all δ_{cp} values.

The precision on the simultaneous measurements of $\sin^2 2\theta_{13}$ and δ_{cp} that can be achieved with a 10 kton detector is shown in Figure 6–19 using different assumptions on signal and background normalization uncertainties. LBNE will be able to measure $\delta_{cp} = 0, \pi/2$ with a precision of $21^\circ, 34^\circ$ assuming $\sin^2 2\theta_{13}$ is externally constrained with an accuracy of 5% - which is the current systematic uncertainty from the Daya Bay experiment. LBNE can also independently measure $\sin^2 2\theta_{13}$ with a precision $\sim 10\%$, which is comparable to the current precision from the reactor experiments.

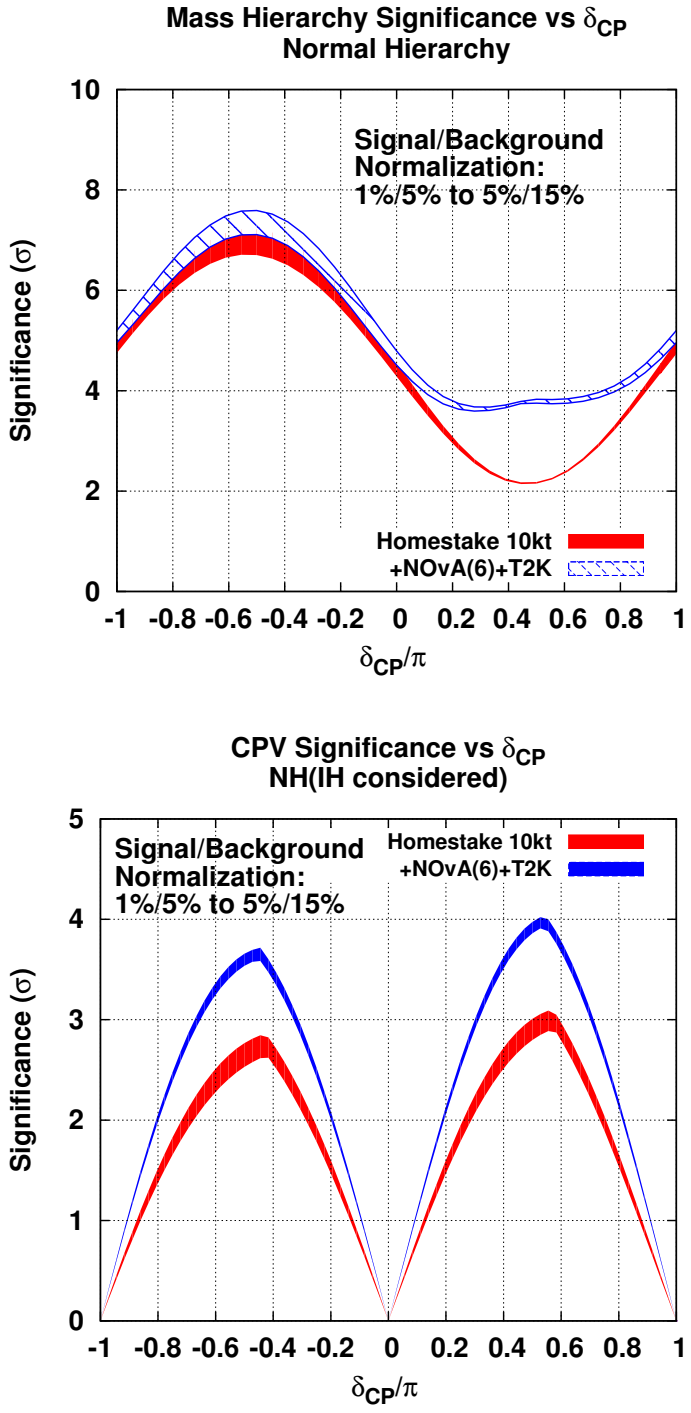

Figure 6–18: The significance with which the mass hierarchy (top) and CP-violation - $\delta_{cp} \neq 0$ or π - (bottom) can be determination as a function of the value of δ_{cp}. The significance is indicated for a 10 kton fiducial volume LAr-FD forfor 5+5 yrs ($\nu + \bar{\nu}$) running in a 708kW beam (6.5×10^{20} protons-on-target/yr). The curves in red show the sensitivity that is achieved by LBNE 10 kton alone. The curves in blue show the sensitivity obtained by combining LBNE 10 kton with T2K and NOνA. The bands indicate the sensitivity range corresponding to different assumptions on background and signal normalization uncertainties.

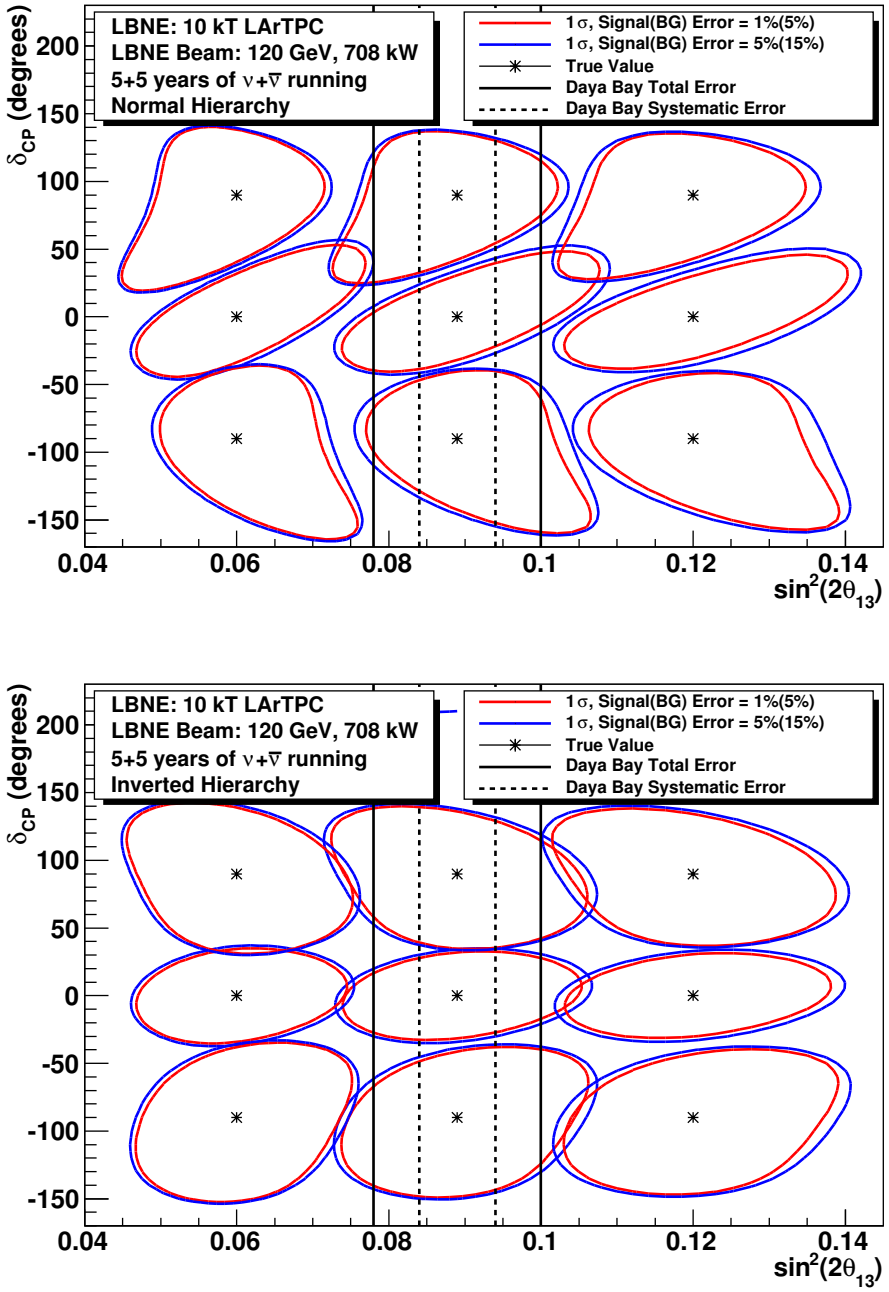

Figure 6–19: Fits to the values of $\sin^2 2\theta_{13}$ and δ_{cp} as a function of $\sin^2 2\theta_{13}$ for normal hierarchy (top) and inverted hierarchy (bottom). The LAr-FD detector mass is assumed to be 10 kton. The uncertainties on the signal/background are varied from 1%/5% (red) to 5%/15% (blue). The dotted and dashed lines represent the current 1σ bounds (dashed = systematics only, dashed = total) on the measurement of $\sin^2 2\theta_{13}$ from the Daya Bay experiment.

6.2.3 Precision Measurements of the Oscillation Parameters in $\nu_\mu \rightarrow \nu_x$ Oscillations

In addition to measurements of ν_e appearance, LBNE can make precise measurements of θ_{23} and $|\Delta m^2_{32}|$ using the $\nu_\mu/\bar{\nu}_\nu$-disappearance channel. Differences in the measured values of $|\Delta m^2_{32}|$ and $|\Delta \bar{m}^2_{32}|$ are sensitive to new physics arising from NC-like non-standard interactions [29] as described in Section 6.2.6.

The expected range of detector performance parameters for the ν_μ-disappearance channel are summarized in Table 6–5. The precision of the measurements of the oscillation parameters and searches for new physics using the $\nu_\mu/\bar{\nu}_\nu$-disappearance channel depends on the accuracy with which the unoscillated spectrum can be estimated using measurements from the near detector complex as well as external measurements and beam simulations.

For the sensitivities estimated here, it is assumed that the unoscillated $\nu_\mu/\bar{\nu}_\mu$ spectrum at the Far Detector can be measured with a 5% normalization uncertainty, and that the NC background can be estimated to within 10%. A detailed discussion of the science and strategy for LBNE with and without a high-precision near detector can be found in [9].

The predicted spectrum of oscillated ν_μ and $\bar{\nu}_\mu$ CC events in LBNE is shown in Figure 6–20.

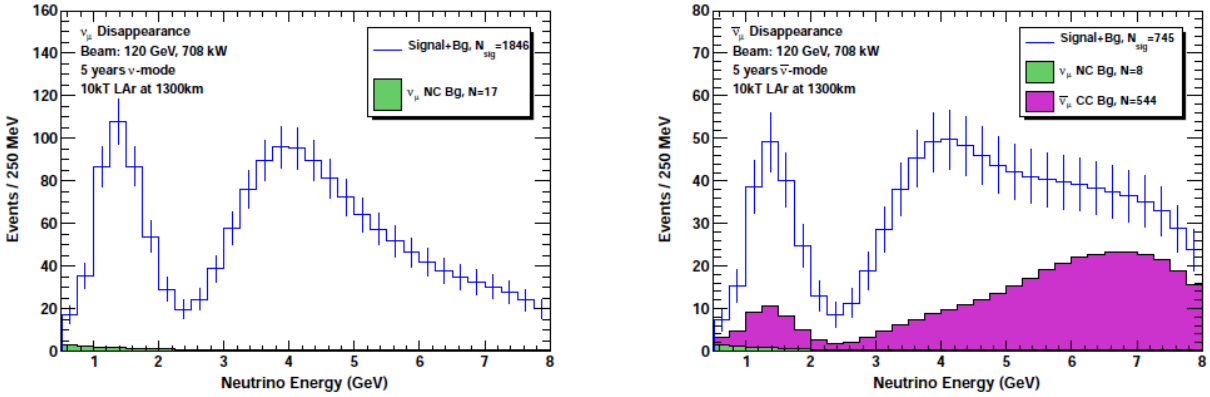

Figure 6–20: The expected spectrum of ν_μ or $\overline{\nu}_\mu$ events in a 10 kton LArTPC for five years of neutrino (left) and antineutrino (right) running with a 700 kW beam, with and without neutrino oscillation.

In Figure 6–21, the result from fits of the expected spectrum of $\nu_\mu/\bar{\nu_\mu}$ CC in the LBNE LAr-FD is shown for different values of Δm^2_{32} and $\sin^2 2\theta_{23}$ for neutrinos and antineutrinos. A $\nu_\mu/\bar{\nu_\mu}$ CC-reconstruction efficiency of 85% and a NC-contamination rate of 0.5% is assumed for these measurements. The signal and background normalization uncertainties are varied from 5-10% for the signal and 10-20% for the background. The larger uncertainties on the

absolute normalization of the signal and background are to chosen to reflect a conservative estimate for how well the absolute flux could be determined using only the muon detectors at the near site. The 10 kton LAr-FD can achieve <2% precision on these parameters assuming the unoscillated ν_μ flux at the Far Detector can be estimated with a precision of 10% or better.

6.2.4 Observation of ν_τ Appearance

The LBNE baseline at 1,300 km will be longer than any long-baseline experiment currently in operation. As a result, ν_μ oscillations occur at higher energy and in particular the energy range is favorable to $\nu_\mu \rightarrow \nu_\tau$ appearance above the τ CC production threshold of 3.2 GeV, as shown in Figure 6–22. In this respect LBNE offers a unique ability compared to current long-baseline experiments in that oscillation between all three flavors of neutrinos could be explicitly observed in a single experiment. To increase the ν_τ CC appearance signal, several high-energy beam tunes produced by moving the target further upstream of LBNE Horn 1 are being considered.

In Table 6–2, ν_τ CC appearance rates for several LBNE beam tunes are shown. The first row in Table 6–2 corresponds to the low-energy beam tune used for the primary oscillation physics analysis. The last two rows correspond to two proposed high-energy beam tunes produced by pulling the target back by 1.5 m and 2.5 m, respectively, from a double parabolic Horn 1. The higher-energy beam tunes can be used to greatly enhance the ν_τ appearance rate. In particular, the medium-energy (ME) tune has high appearance rates for ν_e and ν_τ. It is to be noted that the OPERA experiment which has observed $\nu_\mu \rightarrow \nu_\tau$ appearance in the ν_τ CC mode [30] expects an interaction rate of 2 ν_τ events/1.25 kton/year compared to LBNE which would record a rate of ~ 30 ν_τ events/10 kton/year in the ME beam.

6.2.5 Resolving the θ_{23} Octant

Current experimental results indicate that $\sin^2 2\theta_{23}$ is near maximal ($\sin^2 \theta_{23} = 0.95 \pm 0.02$ [7]), however there exist two solutions of θ_{23} for a given set of measured oscillation parameters, known as the θ_{23} *octant ambiguity*. If the oscillation associated with ν_μ disappearance is not maximal, then it will be important to determine whether θ_{23} is greater than or less than $\pi/4$. This in turn will help show whether the third neutrino mass eigenstate couples more strongly to ν_μ or ν_τ. The value of θ_{23} varies the $\nu_\mu \rightarrow \nu_e$ appearance spectrum as shown in Figure 6–23. The impact of the θ_{23} octant in the energy regions around the second oscillation maximum is very small compared to the effect of δ_{cp} – which is much larger at lower energies – and is the same for neutrinos and antineutrinos, which helps to resolve the degeneracy with the mass hierarchy and δ_{cp} in the region of the first oscillation maximum.

Figure 6–24 displays the capability of LBNE to resolve the θ_{23} octant with a 34 kton LAr-FD

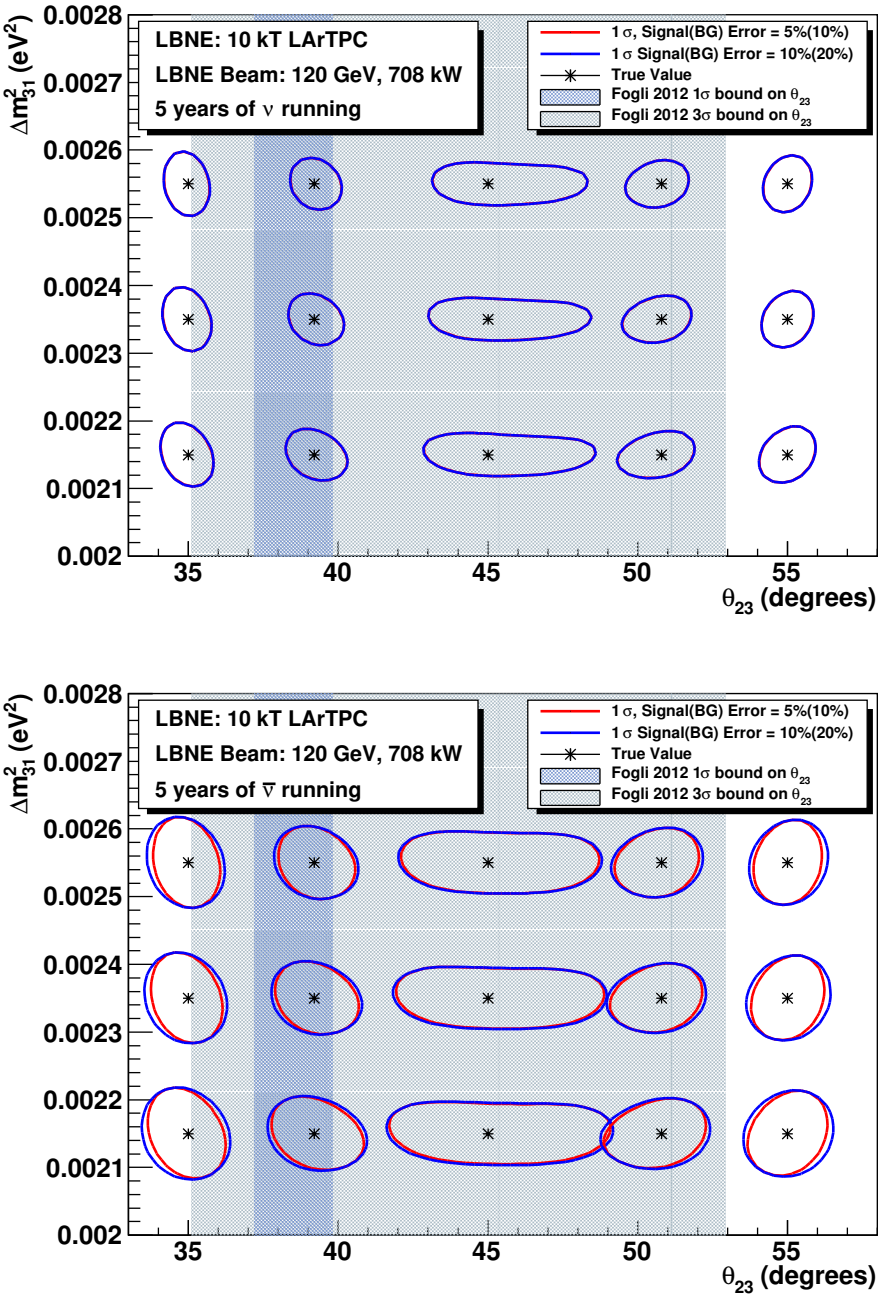

Figure 6–21: Fit to different values of Δm^2_{32} and θ_{23}, for neutrino running (top) and anti-neutrino running (bottom). The LAr-FD detector mass is assumed to be 10 kton. The signal/background normalization uncertainties are assumed to be 5%/10% (red) and 10%/20% (blue). The shaded bands reflect the current 1 and 2 σ uncertainties on θ_{23} obtained from a global fit [7].

running in a 708-kW beam for 10 years or a 10 kton detector running in a 2.3-MW beam for 10 years. The exposure (detector mass $\times$ beam power) assumed for this study is triple

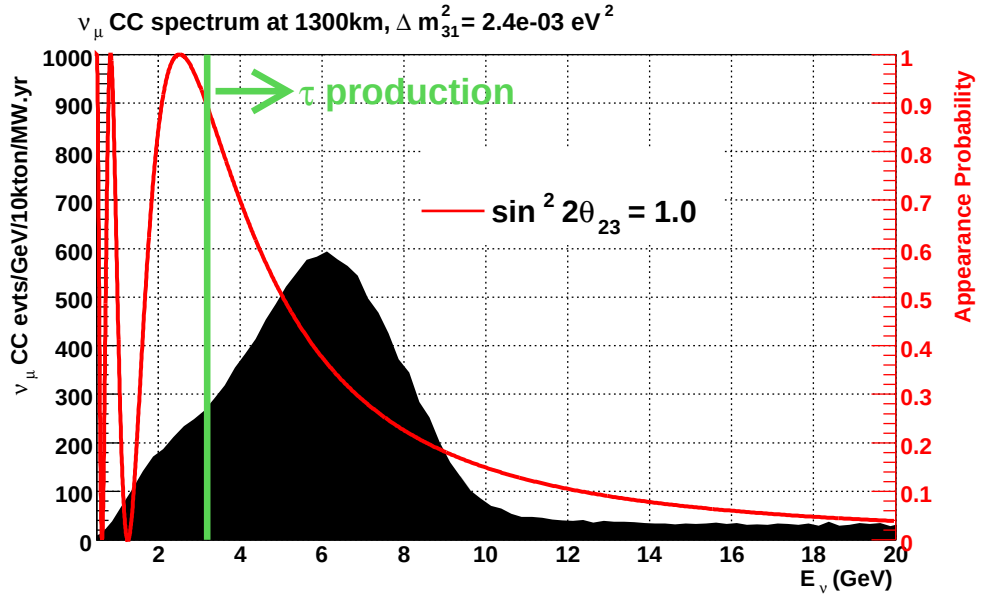

Figure 6–22: The $\nu_\mu \to \nu_\tau$ oscillation probability (red curve) at 1300 km for $\sin^2 2\theta_{23} = 1.0$. The shaded histogram is the unoscillated ν_μ CC spectrum at 1300 km from the medium-energy (ME) beam tune.

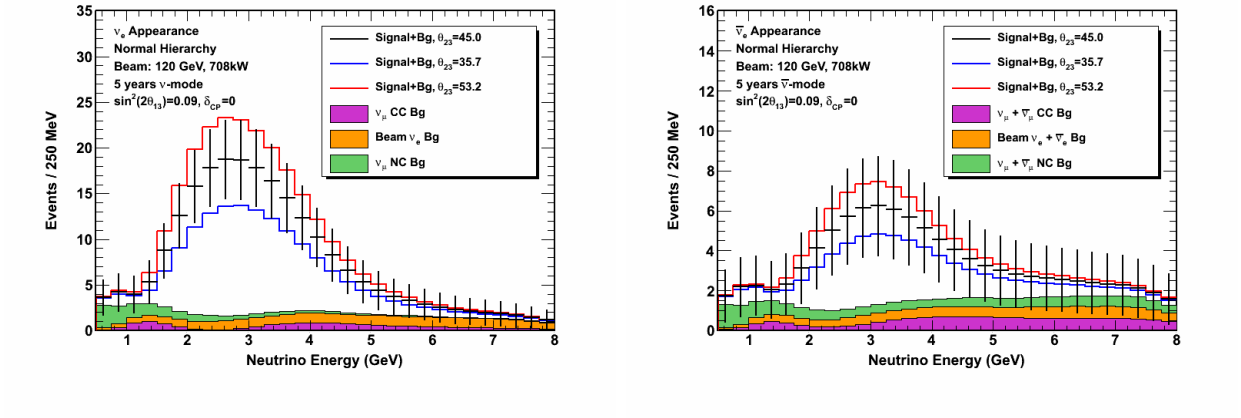

Figure 6–23: The expected spectrum of ν_e or $\overline{\nu}_e$ oscillation events in a 10 kton LArTPC for 5 years of neutrino (left) and antineutrino (right) running with a 708-kW beam, assuming normal hierarchy, $\sin^2(2\theta_{13}) = 0.09, \delta_{cp} = 0$ and varying the value of θ_{23} within the current range of allowed values. Backgrounds are displayed as stacked histograms.

that of the LBNE Project design. For the current best-fit value of $\sin^2 2\theta_{13} = 0.09$, tripling the exposure of LBNE will resolve the θ_{23} octant degeneracy for θ_{23} values less than 41° or greater than 49° at 90% C.L. for 90% of δ_{CP} values. Further improvements in the resolving power of LBNE could be achieved by optimizing the target and focusing in order to produce a greater neutrino flux at lower energies to break degeneracies with δ_{cp} values.

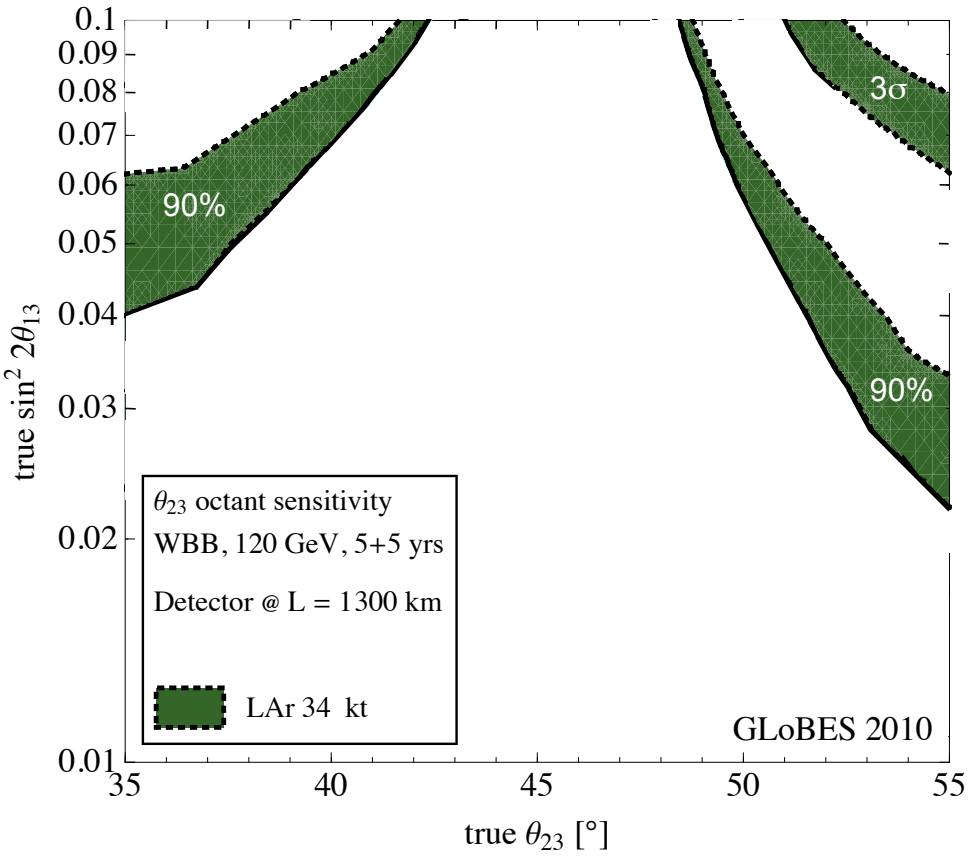

Figure 6–24: Sensitivity of LBNE to resolve the θ_{23} octant degeneracy for 5+5 years of ν+$\bar{\nu}$ running at 700 kW and normal mass hierarchy. The green band shows the results for 34 kton LAr. The width of the bands corresponds to the impact of different true values for δ_{CP}, ranging from a 10% to 90% fraction of δ_{CP}. In the region above the bands, the determination of the θ_{23} octant is possible at 90% CL (lower bands) and 3σ (upper bands).

6.2.6 Searches for New Physics in Long-baseline Oscillations

In addition to precision measurements of the standard three-flavor neutrino-oscillation parameters, the design of LBNE provides the best potential for discoveries of physics beyond the standard three-flavor oscillation model. This section discusses some examples of new physics that the LBNE design is well suited to pursue. It is to be noted that to fully exploit the sensitivity of the LBNE design to new physics will require higher precision predictions of the unoscillated neutrino flux at the Far Detector and larger exposures (detector mass $\times$ beam power) than currently proposed.

6.2.6.1 Non-standard Interactions

NC non-standard interactions (NSI) can be understood as non-standard matter effects that are visible only in a Far Detector at a sufficiently long baseline. LBNE has a unique advantage in this area compared to other long-baseline experiments (except atmospheric-neutrino experiments, which are, however, limited by systematic effects). NC NSI can be parameterized as new contributions to the MSW matrix in the neutrino-propagation Hamiltonian:

$$H = U \begin{pmatrix} 0 & & \\ & \Delta m^2_{21}/2E & \\ & & \Delta m^2_{31}/2E \end{pmatrix} U^\dagger + \tilde{V}_{\rm MSW}\,, \tag{6.1}$$

with

$$\tilde{V}_{\rm MSW} = \sqrt{2} G_F N_e \begin{pmatrix} 1+\epsilon^m_{ee} & \epsilon^m_{e\mu} & \epsilon^m_{e\tau} \\ \epsilon^{m*}_{e\mu} & \epsilon^m_{\mu\mu} & \epsilon^m_{\mu\tau} \\ \epsilon^{m*}_{e\tau} & \epsilon^{m*}_{\mu\tau} & \epsilon^m_{\tau\tau} \end{pmatrix} \tag{6.2}$$

Here, U is the leptonic mixing matrix, and the ϵ-parameters give the magnitude of the NSI relative to standard weak interactions. For new physics scales of few $\times$ 100 GeV, $|\epsilon| \lesssim 0.01$ is expected.

To assess the sensitivity of LBNE to NC NSI, the NSI discovery reach is defined in the following way: After simulating the expected event spectra, assuming given "true" values for the NSI parameters, one attempts a fit assuming no NSI. If the fit is incompatible with the simulated data at a given confidence level, one would say that the chosen "true" values of the NSI parameters are within the experimental discovery reach. Figure 6–25 shows the NSI discovery reach of LBNE for the case where only one of the $\epsilon^m_{\alpha\beta}$ parameters at a time is non-negligible [31]. This calculation assumed a Far Detector mass of 34 kton. With the smaller 10 kton detector, the limits will be less sensitive. Scaling roughly by the expected statistics, LBNE with a 10 kton detector can produce competitive model-independent bounds on NSI in the e–μ sector and significantly improve the bounds in the e–τ sectors by a factor of 2 or 3.

6.2.6.2 Long-range Interactions

The small scale of neutrino-mass differences implies that minute differences in the interactions of neutrinos and antineutrinos with background sources can be detected through perturbations to the time evolution of the flavor eigenstates. The longer the experimental baseline, the higher the sensitivity to a new long-distance potential acting on neutrinos. For example, some of the models for such long-range interactions (LRI) as described in [34] (see Figure 6–26) could contain discrete symmetries that stabilize the proton and a dark matter particle and thus provide new connections between neutrino, proton decay and dark matter

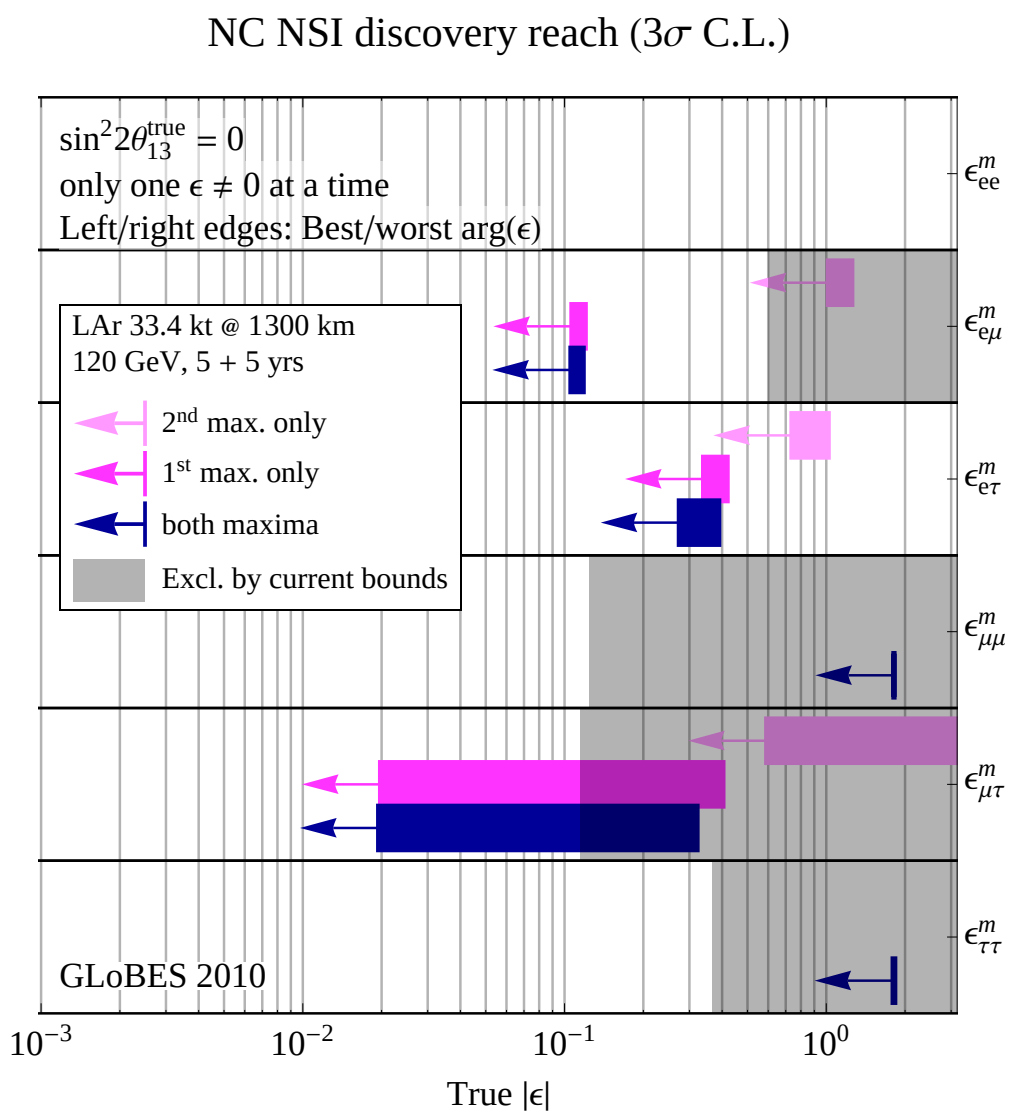

Figure 6–25: Non-standard interaction discovery reach in LBNE with a 34 kton LAr-TPC. The left and right edges of the error bars correspond to the most favorable and the most unfavorable values for the complex phase of the respective NSI parameters. The gray shaded regions indicate the current model-independent limits on the different parameters at 3 σ [32] and [33].For this study the value of $\sin^2 2\theta_{13}$ was assumed to be 0.

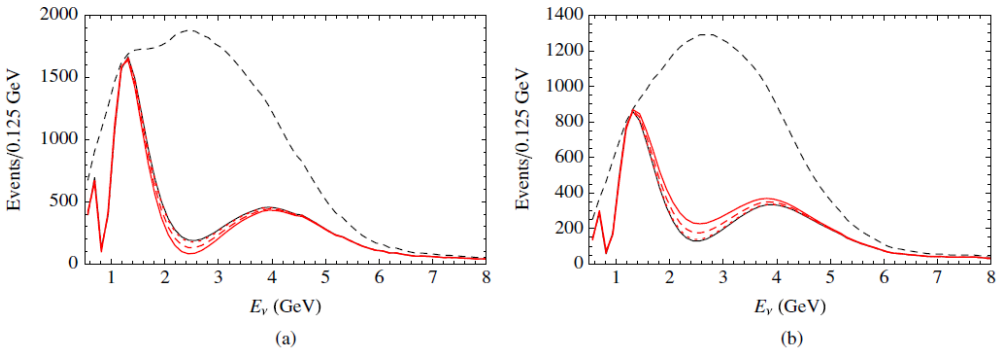

Figure 6–26: Long-range Interactions in LBNE. The number of (a) neutrino and (b) antineutrino events versus E_ν, in a long-baseline experiment with a 1,300-km baseline. The unoscillated case (top black dashed curves) and the case of no new physics (thin black solid curves) are displayed, as well as the cases with $\alpha' = 1.0, 0.5, 0.1 \times 10^{-52}$ corresponding to thick solid, dashed, and dotted curves, respectively. α' is the "fine structure constant" of such interactions which is constrained to be $\alpha' \leq 10^{-47}$ [34].

experiments. The longer baseline of LBNE improves the sensitivity to LRI beyond that possible by the current generation of long-baseline neutrino experiments. The sensitivity will be determined by the amount of $\nu_\mu/\bar{\nu_\mu}$ CC statistics accumulated and the accuracy with which the unoscillated and oscillated ν_μ spectra can be determined. Studies are underway to estimate the sensitivity of the LBNE project to long-range interactions.

6.2.6.3 Search for Active-sterile Neutrino Mixing

Searches for evidence of active-sterile neutrino mixing at LBNE can be conducted by examining the NC event rate at the Far Detector and comparing it to a precision estimate of the expected rate extrapolated from ν_μ flux measurements from the Near Detector Complex and beam and detector simulations. Observed deficits in the NC rate could be evidence for active-sterile neutrino mixing. The latest such search in a long-baseline experiment was conducted by the MINOS experiment [35]. The expected rate of NC interactions with visible energy > 0.5 GeV in LBNE is approximately 1,000 events over five years (see Table 6–2) in the LE beam tune and 3,000 events over five years in the ME beam tune. The NC identification efficiency is high, with a low rate of ν_μ CC background misidentification as shown in Table 6–5. LBNE will provide a unique opportunity to revisit this search with higher precision over a large range of neutrino energies and a longer baseline.

6.2.7 Summary of Accelerator-based Long-Baseline Neutrino Oscillation Measurements

The primary scientific objectives of the LBNE Project are the following:

1. precision measurements of the parameters that govern $\nu_\mu \rightarrow \nu_e$ oscillations, including precision measurements of θ_{13}, measurement of the CP-violating phase δ_{CP} and determination of the mass ordering (the sign of Δm^2_{32})
2. precision measurements of θ_{23} and $|\Delta m^2_{32}|$ in the ν_μ-disappearance channel

Table 6–8 summarizes the expected sensitivity of the LBNE Project to CP-violation in the lepton sector and the neutrino mass ordering and the precision with which θ_{23} and $|\Delta m^2_{32}|$ can be measured. LBNE will significantly improve the sensitivity to CP violation in the neutrino sector beyond that possible by the current generation of experiments (T2K, NOνA). The longer baseline of LBNE will allow an unambiguous determination of the neutrino mass ordering with a $\geq 3\sigma$ significance over 75% of δ_{cp} values. In the small parameter space where CP violating effects and the mass hierarchy are difficult to disentangle in LBNE ($\sim \delta_{cp} = \pi/2(-\pi/2)$ for normal (inverted) hierarchy), combining the measurements of LBNE with the data accumulated by the NOνA and T2K experiment will resolve the degeneracy. LBNE will produce the most competitive measurement of the value of $\sin^2 2\theta_{13}$ from a $\nu_\mu \rightarrow \nu_e$ appearance experiment with a precision comparable to that of the current generation of reactor experiments which measure the parameter using $\bar{\nu_e}$ disappearance. Measurements of θ_{13} with similar precision in both accelerator and reactor experiments over-constrains the three-flavor neutrino oscillation model. LBNE will also measure θ_{23} and $|\Delta m^2_{32}|$ in the ν_μ-disappearance channel with a precision of 1-2% - assuming the unoscillated ν_μ flux can be estimated with an accuracy of 10%. The accuracy of these measurements is comparable to the accuracy expected from the current generation experiments with much shorter baselines. Comparison of oscillation parameter measurements over different baselines will improve sensitivity to new physics that manifests through matter interactions of neutrinos.

The fundamental design of LBNE, with an optimal baseline, a wide-band tunable beam and a high-precision Far Detector, provides a platform for expanding this program in subsequent phases to enable a truly comprehensive investigation of neutrino-oscillation phenomena, which will provide the best potential for discoveries of physics beyond the three-flavor oscillation model. Increasing the detector mass to 34 kton or more, as is allowed by the scalable design of the Far Detector, and increasing the beam power to at least 2.3 MW, as is allowed by the LBNE beam design, will allow full exploitation of this potential.

Table 6–8: Summary of LBNE accelerator-based neutrino oscillation measurements with a 10 kton LAr-FD, running for 5+5 $(\nu + \bar{\nu})$ years in a 708 kW beam. The results summarized here are obtained using the detector performance assumptions listed in the third column of Table 6–5. The mass hierarchy and CP violation sensitivities listed correspond to $\sin^2 2\theta_{13} = 0.092$.

Measurement	Precision
Mass Hierarchy (LBNE 10 kton only) Mass Hierarchy (with T2K)	$> 3\sigma$ for 75% of δ_{cp} values $> 3.5\sigma$ all phase space
CP violation (LBNE 10 kton only) CP violation (with T2K/NoνA)	$> 2.5\sigma$ for 25% of δ_{cp} values $> 3\sigma$ for 40% of δ_{cp} values
δ_{cp} resolution (with external θ_{13} constraint)	$21^\circ(\delta_{cp} = 0),\ 35^\circ(\delta_{cp} = 90^\circ)$
$\sin^2 2\theta_{13}$ resolution	0.01
$\lvert\Delta m^2_{31}\rvert$ resolution	$0.024(\nu),\ 0.034(\bar{\nu}) \times 10^{-3}\text{eV}^2$
θ_{23} resolution	$0.7^\circ(\nu), 1.0^\circ(\bar{\nu})$

6.3 Non-Accelerator Physics that would be Enabled by an Underground Location of the Far Detector

A large liquid argon TPC, when sited underground, has significant capabilities for addressing diverse physics topics, including proton decay, and atmospheric and supernova neutrinos. These capabilities are described in detail in reference [3]. Although the current location of the LBNE LAr-FD near the surface provides insufficient shielding for addressing these physics topics, the LBNE LAr-FD design performance enables a substantially expanded scientific program should it become possible to place it underground either by obtaining additional resources beyond those assumed in the current LBNE Project, or in a later phase of the LBNE program.

For non-beam physics, no external trigger will be available, and therefore a key issue is selection of signal from background, assuming that suitable triggering can be implemented. The photon-detection system included in the LAr-FD design, which detects scintillation light produced by ionizing events, will be a key element of the trigger for non-beam events. Since backgrounds are dominated by cosmic rays, physics reach for a given detector size depends primarily on depth. Table 6–9 summarizes expected signal rates. Proton decay and atmospheric neutrino events are, like beam events, ∼GeV scale, and should in principle be quite cleanly identifiable in an LArTPC; see Figures 6–27 and 6–28. Proton-decay events, although distinctive, would be extremely rare, and hence highly intolerant of background; in contrast, atmospheric neutrinos (which are background for proton decay) have a higher rate and could tolerate some background. The signatures of individual supernova-burst neutrino interaction events are much less clean. With only a few tens of MeV of energy, these neutrinos will create small tracks involving only a few adjacent wires; see Figure 6–29. For diffuse "relic" supernova events which arrive singly, the very low expected signal rate makes their selection

overwhelmingly difficult, and they are not considered further here. A nearby core collapse is more promising; it will provide a pulse of low-energy events all arriving within ∼30 seconds, so that LBNE can hope to make a meaningful measurement of signal over a (well-known) background.

Table 6–9: Expected signal rates of non-beam processes whose detection would be enabled by placing the LBNE Far Detector underground. The supernova-burst event rate is the average over the ≈ 30second interval of the occurrence for a supernova at 10 kpc.

Physics	Energy range	Expected signal rate (events kton^{-1}s^{-1})
Proton decay	$\sim$ GeV	$< 2 \times 10^{-9}$
Atmospheric neutrinos	$0.1 - 10$ GeV	$\sim 10^{-5}$
Supernova burst neutrinos	few-50 MeV	~ 3
Diffuse supernova neutrinos	20-50 MeV	$< 2 \times 10^{-9}$

The physics reach will be considered as a function of detector mass and depth for proton decay, supernova bursts and atmospheric neutrinos. (Solar neutrinos will not be considered; with mostly <10 MeV energies, they require stringent control of background. Other than providing a ν_e calibration in argon for supernova neutrinos, they are not likely to tell us anything not already known in the detectors under consideration.)

6.3.1 Searches for Baryon Number Non-conservation

Searches for baryon-number-violating processes are highly motivated by grand unified theories. Even a single event could be evidence of physics beyond the Standard Model. Current limits are dominated by Super–Kamiokande [37]; however for some predicted modes, most prominently $p \to K^+\bar{\nu}$, efficiency for water Cherenkov detectors is low, and detectors that can cleanly reconstruct kaon decay products have a substantial efficiency advantage. Other modes for which LArTPCs have an edge include $n \to e^- K^+$ and $p \to e^+\gamma$. Figure 6–30 shows the expected limit as a function of time for $p \to K^+\bar{\nu}$. According to this plot, approximately 10 kton of LAr is required to improve the limits significantly beyond continued Super–Kamiokande running.

In LAr, the most pernicious background for proton decay with kaon final states comes from cosmic rays that produce entering kaons in photonuclear interactions in the rock near the detector. Backgrounds as a function of depth have been studied for LAr in references [36,38,39]. These studies show that proton decay searches can be successful at moderate depth at the expense of a reduction of fiducial mass or in conjunction with a high-quality veto, but cannot be done at the surface. The 4850L at SURF would be an excellent location and would not require an external veto system.

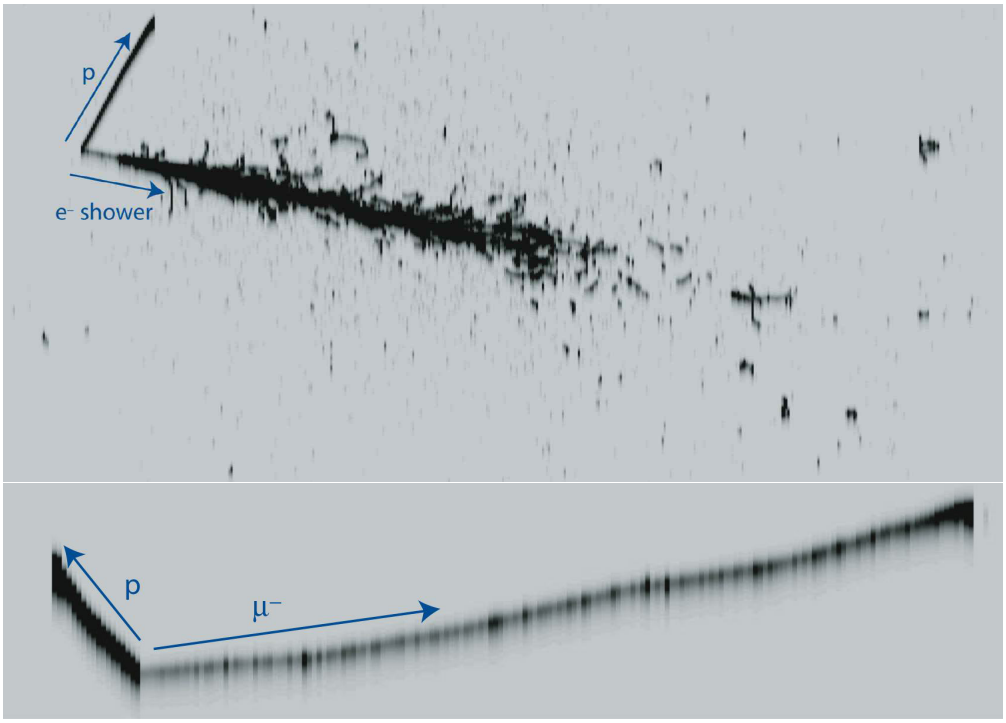

Figure 6–27: Simulated ν_e and ν_μ CC atmospheric neutrino events in liquid argon from reference [36].

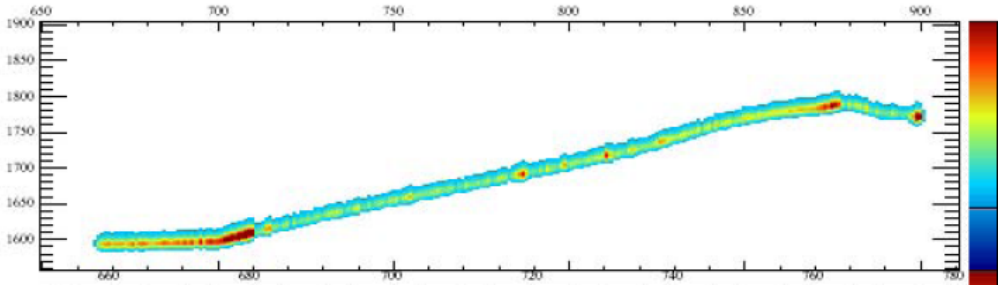

Figure 6–28: LArSoft simulation of $p \to K^+\bar{\nu}$ decay with $K^+ \to \mu^+ \to e^+$ in the MicroBooNE geometry. The drift time is along the vertical axis. The wire number is along the horizontal axis (3-mm wire spacing). The color indicates amount of charge deposited (red is larger, blue smaller).

6.3.2 Atmospheric Neutrinos

Atmospheric neutrinos are unique among sources used to study oscillations: the oscillated flux contains neutrinos and antineutrinos of all flavors, and matter effects play a significant role. The expected interaction rate is about 285 events per kton-year. The excellent CC/NC separation and the ability to fully reconstruct the hadronic final state in CC interactions in an LArTPC would enable the atmospheric neutrino 4-momentum to be fully reconstructed. This would enable a higher-resolution measurement of L/E to be extracted from atmospheric-neutrino events in an LArTPC compared to the measurements obtained

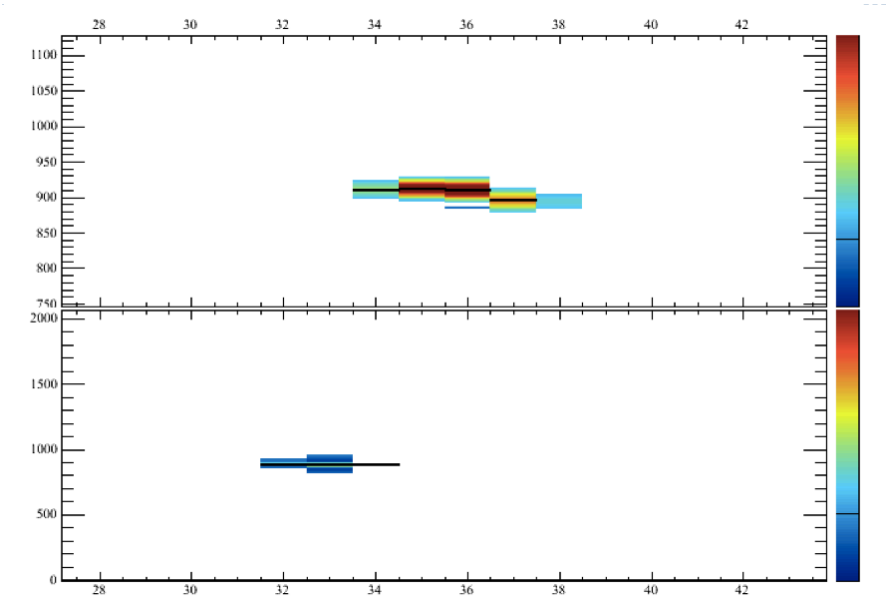

Figure 6–29: LArSoft simulation of a 10 MeV electron (which would resemble a supernova-neutrino event) in the MicroBooNE geometry (3-mm wire spacing). There are four reconstructed hits (black bands) on five adjacent wires. This event would create signals on about four wires with 5-mm spacing. The drift time is on the vertical axis, and the wire number is on the horizontal axis.

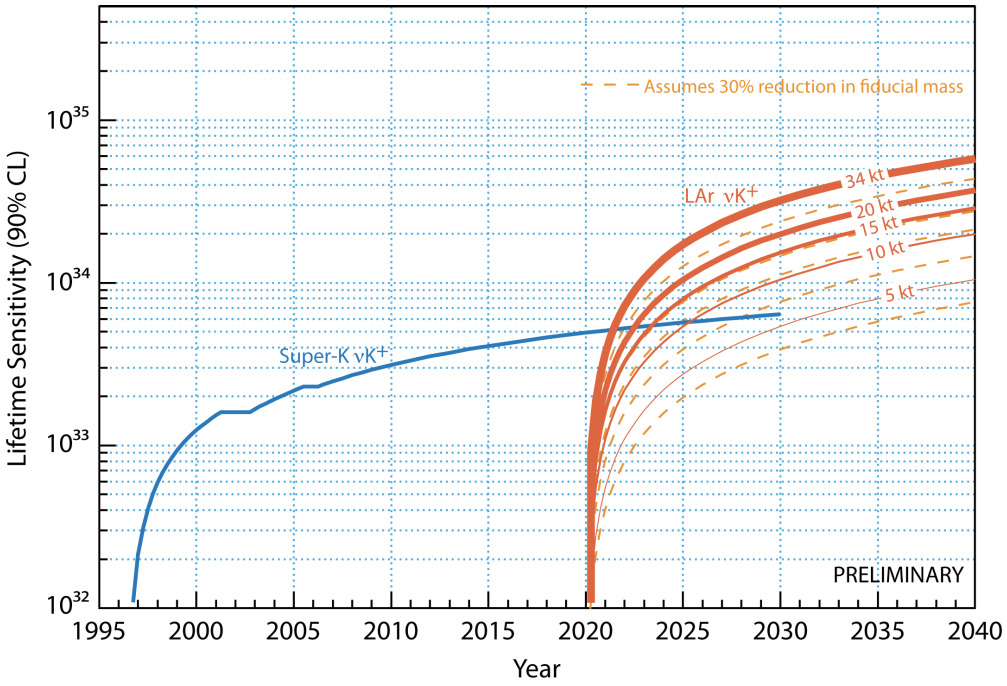

Figure 6–30: Proton decay lifetime limit for $p \rightarrow K^{+}\bar{\nu}$ as a function of time for Super–Kamiokande compared to different LAr masses at the 4850 level SURF starting in 2020. The dashed lines show the effect of a 30% reduction of fiducial mass, conservatively assumed for a shallower depth of 2300 feet. The limits are at 90% C.L., calculated for a Poisson process including background assuming that the detected events equal the expected background. (Figure from J. Raaf.)

from Super–Kamiokande, and would provide good sensitivity to mass hierarchy and to the octant of θ_{23}. Since the oscillation phenomenology plays out over several decades in energy and path length, atmospheric neutrinos are very sensitive to alternative explanations or subdominant new physics effects that predict something other than the characteristic L/E dependence predicted by oscillations in the presence of matter.

Because atmospheric neutrinos are somewhat more tolerant of background than proton decay, a depth that is sufficient for a proton decay search should also be suitable for atmospheric neutrinos. For the SURF 4850L depth, a veto should not be necessary, and one can assume full fiducial mass; at depths around 2,700 feet, a one-meter fiducial cut should be adequate. Figure 6–31 shows expected sensitivity to mass hierarchy; for ten years of running, even a 10 kton detector would add to world knowledge.

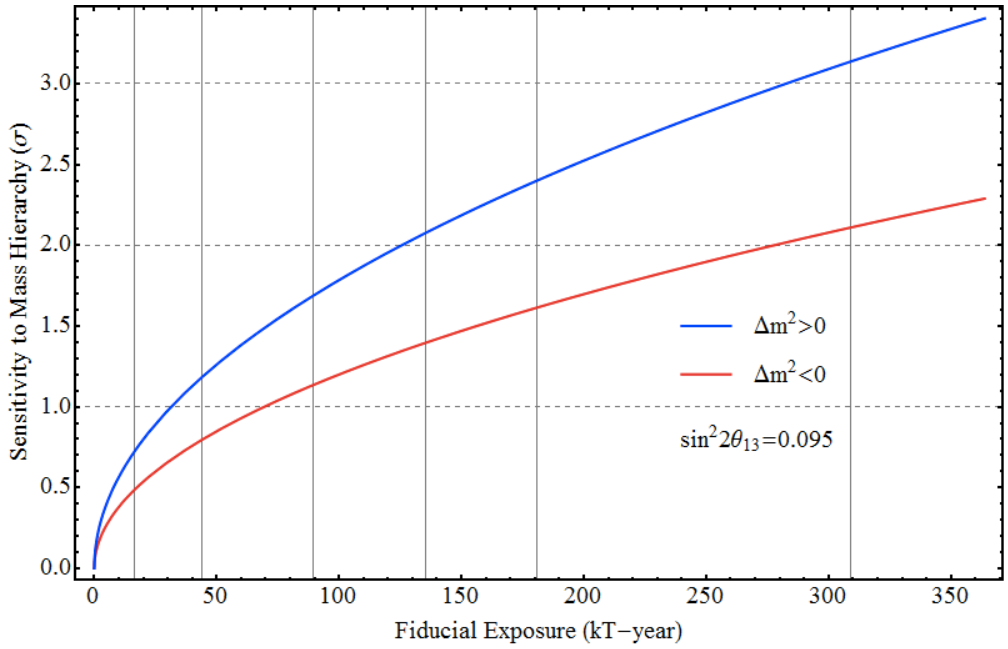

Figure 6–31: Sensitivity to mass hierarchy using atmospheric neutrinos as a function of fiducial exposure in a LAr detector. (Figure from H. Gallagher, J. Coelho, A. Blake.)

6.3.3 Core-Collapse Supernova Neutrinos

A nearby core-collapse supernova will provide a wealth of information via its neutrino signal (see [40,41] for reviews). The neutrinos are emitted in a burst of a few tens of seconds duration. Energies are in the few tens of MeV range, and luminosity is divided roughly equally between flavors. Ability to measure and tag the different flavor components of the spectrum is essential for extraction of physics and astrophysics from the signal. Currently, world-wide sensitivity is primarily to electron anti-neutrinos, via inverse beta decay on free protons, which dominates the interaction rate in water and liquid scintillator detectors. LAr

has a unique sensitivity to the *electron neutrino* component of the flux, via the absorption interaction on ^{40}Ar, $\nu_e + {}^{40}\mathrm{Ar} \rightarrow e^- + {}^{40}\mathrm{K}^*$. In principle, this interaction can be tagged via the de-excitation gamma cascade. About 900 events would be expected in the 10 kton fiducial mass of the LAr-FD for a supernova at 10 kpc; the number of signal events scales with mass and the inverse square of distance as shown in Figure 6–32. For a collapse in the Andromeda galaxy, a 34 kton detector would expect about one event. This sensitivity would be lost for the smaller 10 kton detector. However the 10 kton detector would gather a unique ν_e signal from within the Milky Way.

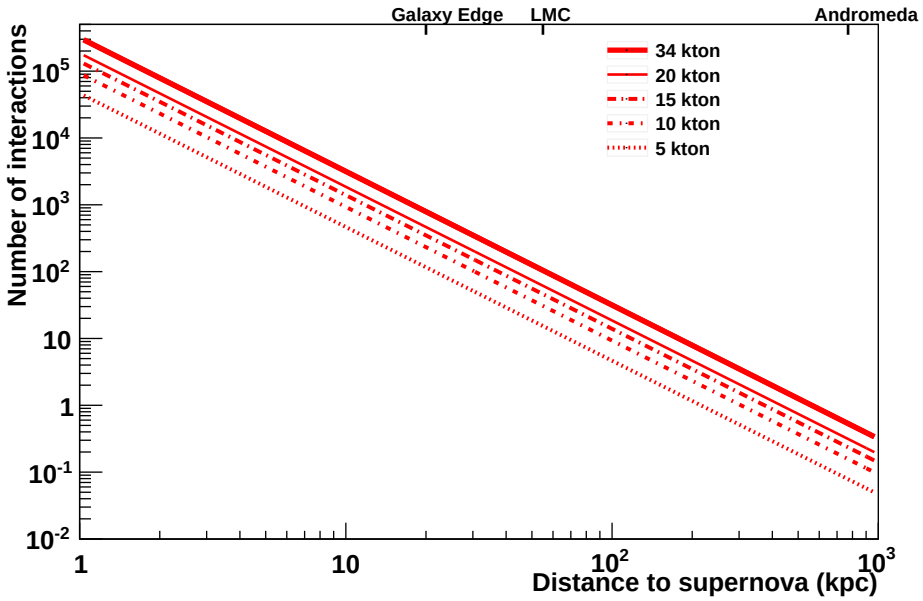

Figure 6–32: Number of supernova neutrino interactions in a LAr detector as a function of distance to the supernova, for different detector masses. Core collapses are expected to occur a few times per century, at a most-likely distance of about 10-15 kpc.

As noted above, due to their low energy, supernova events are subject to background, although the short-timescale-burst nature of the signal means that the background can be well known and subtracted. Muons and their associated Michel electrons can in principle be removed. Radioactive decays, including cosmogenic spallation products, tend to make <10 MeV signals. They lie below the main supernova signal range, but inhabit a potential region of interest for physics signatures. Preliminary studies from reference [28], extended for cosmic-ray rates on the surface, suggest that while the 4850L depth is acceptable, the surface cosmic-ray-associated signal rates are daunting. It will require at least a few orders of magnitude of background rejection to pull the signal from background. While more work needs to be done to determine the extent to which the background can be mitigated, a surface option is highly unfavorable for supernova-neutrino physics.

6.3.4 Summary

Although more work needs to be done to understand backgrounds at shallow depth, the following findings are fairly robust:

- Proton decay capabilities as a function of depth are quite well documented, and a search at the surface seems impossible. A detector mass of at least 10 kton would be needed for competitiveness.
- For atmospheric neutrinos, less is known about signal selection on the surface; however it is probably extremely difficult. The 4850L depth at SURF is highly acceptable. Underground, a 20 kton detector would be needed for competitiveness, although a 10 kton detector could still provide useful information.
- For supernova-burst neutrinos, selection of signal events over background at the surface will be a daunting task, and information will be highly degraded even in the best case. The 4850L depth at SURF is acceptable. More mass is always better, but even a 5 kton detector would provide a unique ν_e-flavor supernova signal.

In summary, a reasonably-sized LAr detector $\geq$ 10 kton sited at the 4850L at SURF would provide excellent opportunities for a diverse range of physics topics. At the current shallow location for the LBNE LAr-FD, capabilities for non-beam physics are extremely poor.

References

[1] J. Appel *et al.*, "Physics Working Group Report to the LBNE Reconfiguration Steering Committee," 2012. http://www.fnal.gov/directorate/lbne_reconfiguration/files/LBNE-Reconfiguration-PhysicsWG-Report-August2012.pdf.

[2] Y. K. Kim *et al.*, "LBNE Reconfiguration: Steering Committee Report," 2012. http://www.fnal.gov/directorate/lbne_reconfiguration/index.shtml.

[3] T. Akiri *et al.*, "The 2010 Interim Report of the Long Baseline Neutrino Experiment Collaboration Physics Working Groups." arXiv:1110.6249.

[4] T. Katori, "MicroBooNE, A Liquid Argon Time Projection Chamber (LArTPC) Neutrino Experiment." arXiv:1107.5112 [hep-ex], 2011.

[5] LBNE Science Collaboration, "LBNE Case Study Report, Liquid Argon TPC Far Detector, Draft Version 1.2," 2011.

[6] J. Beringer *et al.*, "Review of Particle Physics," *Phys.Rev.D.*, vol. 86, p. 010001, 2012.

[7] G. Fogli *et al.*, "Global analysis of neutrino masses, mixings and phases: entering the era of leptonic CP violation searches," *Phys.Rev.D.*, vol. 86, p. 013012, 2012.

[8] S. Agostinelli *et al.*, "GEANT4 — A Simulation Toolkit," *Nucl. Instrum. Methods*, vol. A, no. 506, pp. 250–303, 2003.

[9] M.Bishai *et al.*, "The Science and Strategy for a Long-Baseline Neutrino Experiment," 2012. http://www.fnal.gov/directorate/lbne_reconfiguration/index.shtml.

[10] P. Adamson *et al.*, "Improved search for muon-neutrino to electron-neutrino oscillations in MINOS," *Phys. Rev. D.*, vol. 77, p. 072002, 2008.

[11] L. Loiacono, *Measurement of the muon neutrino inclusive charged current cross section on iron using the MINOS detector*. PhD thesis, University of Texas, Austin, 2010.

[12] B. Osmanov, "MINERvA Detector: Description and Performance." arXiv:1109.2855 [hep-ex], 2011.

[13] A. Ferrari *et al.*, "FLUKA: a multi-particle transport code," 2005.

[14] G. Battistoni *et al.*, "The FLUKA code: Description and benchmarking," *AIP Conference Proceeding*, vol. 896, p. 31, 2007.

[15] M. Makariev, "Pion production in p + C collisions at 158-GeV/c beam momentum.," *AIP Conf.Proc.*, vol. 899, p. 203, 2007.

[16] N. Abgrall *et al.*, "Measurements of Cross Sections and Charged Pion Spectra in Proton-Carbon Interactions at 31 GeV/c," *Phys.Rev.*, vol. C84, p. 034604, 2011.

[17] R. Raja, "The main injector particle production experiment (MIPP) at Fermilab," *Nucl. Instrum. Meth.*, vol. A553, pp. 225–230, 2005.

[18] S. Kopp *et al.*, "Secondary beam monitors for the NuMI facility at FNAL," *Nucl. Instrum. Meth. A*, vol. 568, p. 503, 2006.

[19] The LArSoft Collaboration. `https://plone4.fnal.gov:4430/P1/Main/wiki/LArSoft/LArSoft`.

[20] T2K Collaboration, "Proposal to Extend T2K with a detector 2km Away from the JPARC Neutrino Source," 2007. `http://neutrino.cgi.phy.duke.edu/2km/wiki/index.cgi/`.

[21] "A Large Liquid Argon Time Projection Chamber for Long-baseline Off-Axis Neutrino Oscillation Physics with the NuMI Beam," tech. rep., 2005. Submitted to the NuSAG committee; inspirehep.net FERMILAB-FN-0776-E.

[22] B. Baller *et al.* tech. rep. LBNE-doc-266-v1, LBNE-doc-3414-v2.

[23] J. Raaf *et al.*, "LAr Hand Scan," tech. rep., FNAL, IMsA, 2012. LBNE-doc-5446.

[24] `http://icarus.lngs.infn.it/`.

[25] P. Adamson *et al.*, "Improved search for muon-neutrino to electron-neutrino oscillations in MINOS," *Phys. Rev. Lett.*, vol. 107, p. 181802, 2011.

[26] S.Amoruso *et al. Eur. Phys. J.*, vol. C33, p. 233, 2004.

[27] A. Ankowski *et al.*, "Measurement of through-going particle momentum by means of multiple scattering with the icarus t600 tpc.," *Eur. Phys. J.*, vol. C48, p. 667, 2006.

[28] D. Barker *et al.*, "Muon-induced background for beam neutrinos at the surface," 2012. `http://www.fnal.gov/directorate/lbne_reconfiguration/index.shtml`.

[29] W. A. Mann *et al.*, "Apparent multiple Δm^2_{32} in muon anti-neutrino and muon neutrino survival oscillations from non-standard interaction matter effect," *Phys. Rev. D.*, vol. 82, p. 113010, 2010.

[30] U. Kose, "Search for $\nu_\mu \to \nu_\tau$ oscillations in appearance mode in the OPERA experiment.." arXiv:1106.3871 [hep-ex], 2011.

[31] P. Huber and J. Kopp, "Two experiments for the price of one? The role of the second oscillation maximum in long baseline neutrino experiments." arXiv:1010.3706, 2011.

[32] S. Davidson, C. Pena-Garay, N. Rius, and A. Santamaria hep-ph/0302093, 2003.

[33] M.C. Gonzalez-Garcia, and M. Maltoni, "Phenomenology with Massive Neutrinos," *Phys. Rept.*, vol. 460, p. 1, 2008. arXiv:0704.1800 [hep-ph].

[34] H. Davoudiasl *et al.*, "Long-Range Lepton Flavor Interactions and Neutrino Oscillations.," *Phys. Rev. D.*, vol. 84, p. 013009, 2011. arXiv:1102.5352 [hep-ph].

[35] P. Adamson *et al.*, "Search for sterile neutrino mixing in the MINOS long baseline experiment," *Phys. Rev. D.*, vol. 81, p. 052004, 2010. arXiv:1001.0336 [hep-ex].

[36] A. Bueno, A. J. Melgarejo, S. Navas, Z. D. ai, Y. Ge, M. Laffranchi, A. M. Meregaglia, and A. Rubbia, "Nucleon decay searches with large liquid Argon TPC detectors at shallow depths: atmospheric neutrinos and cosmogenic backgrounds," *Journal of High Energy Physics*, vol. 2007, no. 04, p. 041, 2007.

[37] H. Nishino, S. Clark, *et al.*, "Search for Proton Decay via $p \to e^+\pi^0$ and $p \to \mu^+\pi^0$ in a Large Water Cherenkov Detector," *Phys. Rev. Lett.*, no. 102:141801, 2009. arXiv:0903.0676 [hep-ex].

[38] A. Bernstein *et al.*, "Report on the Depth Requirements for a Massive Detector at Homestake (LBNE:DocDB-34)," 2009. arXiv:0907.4183 [hep-ex].

[39] V. Kudryavtsev *et al.*, "Cosmic rays and cosmogenics. report to the lbne collaboration.," tech. rep., 2012. LBNE-doc-5904.

[40] K. Scholberg, "Supernova neutrino detection," *Nucl.Phys.Proc.Suppl.*, vol. 221, p. 248, 2011. astro-ph/0701081.

[41] A. Dighe, "Physics potential of future supernova neutrino observations," *J.Phys.Conf.Ser.*, vol. 136, p. 022041, 2008. arXiv:0809.2977 [hep-ph].